Engineering Geology 367 (2026) 108648

Contents lists available at ScienceDirect

Engineering Geology

journal homepage: www.elsevier.com/locate/enggeo

# Formation, propagation, and annihilation of surge waves in debris flows☆

Christoph Wetter [a,c,*], Fabian Walter [a], Brian W. McArdell [a], Felix Blumenschein [a], Raffaele Spielmann [a,b], Jordan Aaron [a,b], J.M.N.T. Gray [d], Anne Obermann [e], Andreas Fichtner [c]

[a] Swiss Federal Institute for Forest, Snow and Landscape Research (WSL), Zürcherstrasse 111, Birmensdorf, 8903, Switzerland
[b] Chair of Engineering Geology, Geological Institute, Department of Earth and Planetary Sciences, ETH Zürich, Sonneggstrasse 5, Zurich, 8092, Switzerland
[c] Institute of Geophysics, Department of Earth and Planetary Sciences, ETH Zürich, Sonneggstrasse 5, Zurich, 8092, Switzerland
[d] Department of Mathematics and Manchester Centre for Nonlinear Dynamics, The University of Manchester, Oxford Road, Manchester, M13 9PL, United Kingdom
[e] Swiss Seismological Service (SED), ETH Zürich, Sonneggstrasse 5, Zurich, 8092, Switzerland

ARTICLE INFO

*Keywords:*
Debris flows
Seismic monitoring
Surge waves
Roll waves
Erosion-deposition waves
Hazard assessment
Structural measures

ABSTRACT

In recent years, the destructive impact of debris flows in alpine regions has become increasingly evident. Surge waves within debris flows increase peak discharge and magnify the hazard potential. Hence, understanding the dynamic complexity of debris flows is crucial to mitigate their risk. In order to capture the dynamic processes involved in the formation and interaction of surge waves, it is necessary to obtain distributed observations in the spatiotemporal domain. In this study, we present near-torrent distributed seismic measurements to monitor the Illgraben channel located in the Swiss Alps. With 33 nodal sensors, we detected and tracked surge waves along a 2-km torrent section across the Illgraben fan. This provided valuable new insights into the spatial scales relevant for surge wave formation and the long-distance propagation characteristics from surge wave formation to their annihilation. We observed erosion-deposition waves that emerged out of the muddy flow tail and propagated with constant velocity along the torrent, reaching meter-scale flow heights within only hundreds of meters of flow distance. We can differentiate flow regimes based on their seismic signature and track them along the torrent, thus mapping the debris-flow evolution in time and space. The observations elucidate large-scale debris flow dynamics and improve our understanding of hazard potential and the effectiveness of structural countermeasures.

## 1. Introduction

Debris flows are fast-moving, surging mixtures of sediment and water (Iverson et al., 1997), which episodically move down steep mountain torrents, typically triggered by extreme precipitation events (Berti et al., 2000) or snow melt (Mostbauer et al., 2018). They belong to a range of alpine mass movements that continuously reshape the Earth's surface by displacing large quantities of sediment over short time scales. Debris flows have high destructive potential, as their volumes often exceed tens of thousands of cubic meters, and their velocity can surpass 5 m/s (Zanuttigh and Lamberti, 2007). Debris flows typically evolve into sequences of surges (Zanuttigh and Lamberti, 2007; Arai et al., 2013; McArdell, 2016; Chen et al., 2024) and as volumetric sediment concentrations exceed 40%, complex fluid-solid mechanics are observed (Iverson et al., 1997). Flow instabilities can lead to the formation of quasi-periodic waves in flow height with amplitudes that may exceed 1 meter (e.g., Costa and Williams, 1984; Zanuttigh and Lamberti, 2007; McArdell, 2016; Schöffl et al., 2023; Chen et al., 2024; Aaron et al., 2025) often referred to as surge waves. Surge waves are much more destructive than a steady uniform flow with the same mass flux, due to their higher peaks in flow height, velocity, and discharge (Aaron et al., 2025) and the ability to transport large boulders (Spielmann et al., 2025). Hence, a detailed understanding of the emergence and propagation of surge waves is needed to better manage the hazard associated with surging debris flows and design structural countermeasures.

### 1.1. Surge waves within debris flows

Surge-like waves in granular gravity-driven flows are widely observed in nature, e.g., debris flows (McArdell, 2016), mud flows (Balmforth and Liu, 2004), snow avalanches (Edwards et al., 2017; Li et al., 2024) and even granular avalanches on the moon (Kokelaar et al.,

☆ This article is part of a Special issue entitled: 'Debris flow mitigation' published in Engineering Geology.

* Corresponding author at: Swiss Federal Institute for Forest, Snow and Landscape Research (WSL), Zürcherstrasse 111, Birmensdorf, 8903, Switzerland.
*E-mail address:* christoph.wetter@wsl.ch (C. Wetter).

https://doi.org/10.1016/j.enggeo.2026.108648
Received 9 September 2025; Received in revised form 19 December 2025; Accepted 28 February 2026
Available online 25 March 2026

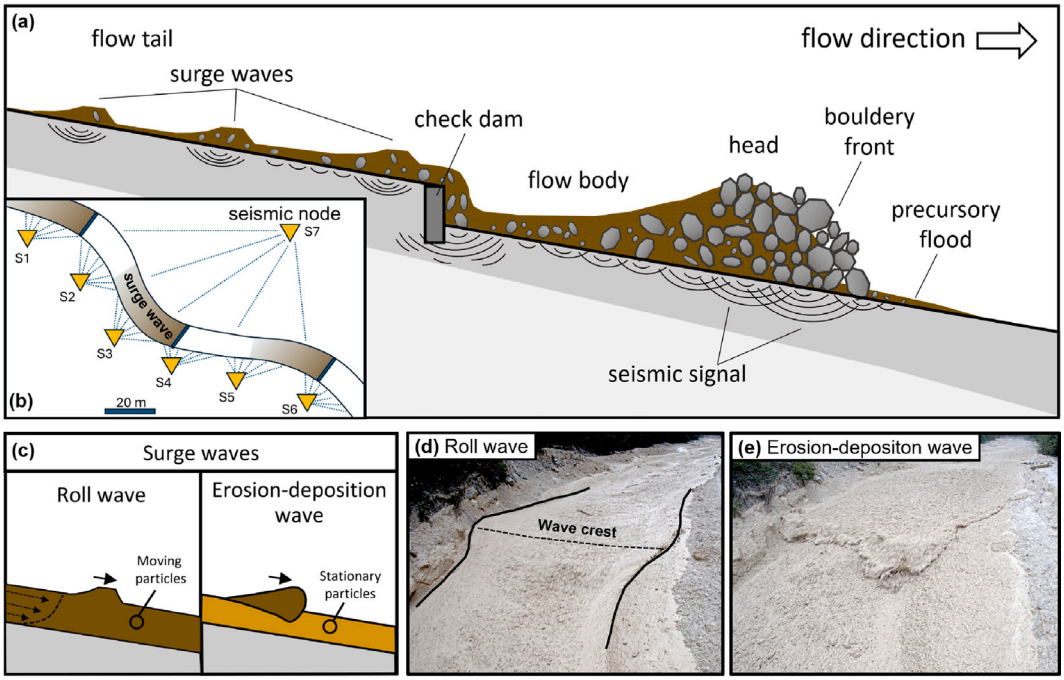


**Fig. 1.** (a) Conceptual illustration of debris flow. Seismic signals (1–100 Hz) are predominantly generated by boulder-ground impacts of material transported in the flow. (b) Plan view illustration of seismic array. Dense near-torrent seismic arrays are required to resolve passing flow surges (nodes S1-S6). In case of seismic node S7 only the integrated seismic signal of a large torrent section is recorded. (c-e) Two types of surge waves: Roll waves and erosion-deposition waves. Erosion-deposition waves are alternating regions of static and mobile sediment whereas roll waves propagate within a fully mobilized flow.

2017). Two types of surge waves are particularly relevant for debris flows: (1) roll waves (e.g., McArdell, 2016) and (2) erosion-deposition waves (Costa and Williams, 1984; Edwards and Gray, 2015; Schöffl et al., 2023; Chen et al., 2024). In Fig. 1 both wave types are illustrated.

Roll waves arise spontaneously from small flow perturbations due to the roll wave instability, first analyzed by Jeffreys (1925), which is driven by a force feedback of gravity and friction of the flowing material (Aaron et al., 2025). Numerical studies and laboratory experiments by Razis et al. (2014) and Viroulet et al. (2018) showed that large roll waves travel faster than small ones, resulting in the merging and growth of individual waves during runout.

Erosion-deposition waves can occur in materials that exert an effective yield stress (Edwards and Gray, 2015), such as dry-granular flows (Daerr, 2001; Rocha et al., 2019; Edwards et al., 2021) or debris flows (e.g., Schöffl et al., 2023) forming finite-length waves with static regions in between. The static material in front of the wave becomes eroded, transported with the wave, and eventually deposited at the base, sides, and tail of the wave (Edwards et al., 2017). Two different formation mechanisms of erosion-deposition waves have been discussed: (1) Roll wave instability in the case of continuous inflow conditions (Edwards and Gray, 2015; Aaron et al., 2025), and (2) frictional-hysteresis in the case of static inflow conditions (Edwards et al., 2017). Laboratory-scale studies and theoretical models (Takagi et al., 2011; Edwards et al., 2017; Rocha et al., 2019; Edwards et al., 2021) suggest that large-scale erosion-deposition waves within debris flows can form steady-traveling-states of erosion and deposition and therefore propagate indefinitely along the torrent as long as the erodible layer ahead of the wave does not change depth and the inclination remains the same (Edwards et al., 2017).

In order to capture the dynamic processes involved in the formation, evolution and long distance propagation of surge waves within debris flows, it is necessary to obtain distributed observations of full scale debris flows in the spatiotemporal domain on kilometer distance scales (Aaron et al., 2025). Most field observations of surge waves have been restricted to point measurements (e.g. Zanuttigh and Lamberti, 2007) or small torrent sections using pulse-Doppler radar (Schöffl et al., 2023) or 3D LiDAR scanners (Aaron et al., 2023, 2025). Demanding field installations have confined quantitative and systematic studies to numerical or laboratory settings (e.g. Fraccarollo and Papa, 2000; Daerr, 2001; Razis et al., 2014; Edwards and Gray, 2015; Edwards et al., 2017; Viroulet et al., 2018; Rocha et al., 2019) and results have not been validated for full-scale debris flows.

### 1.2. Environemental seismology

Environmental seismology provides an alternative method for investigating the propagation of debris flow surges and surge waves, although until now such experiments have been limited to relatively few sensors and hence short torrent sections (Arattano and Moia, 1999; Navratil et al., 2013; Coviello et al., 2019) or flume experiments (e.g. Allstadt et al., 2020). Stochastic single-particle-ground impacts (Farin et al., 2019; Lai et al., 2018) or multi-particle force chains (Zhang et al., 2021a) are considered the primary source of high frequency signals (1–100 Hz), with large boulders dominating the seismogenesis of debris flows (Farin et al., 2019; Zhang et al., 2021b). Physical models typically link frequency content and signal strength with particle size distribution, particle impact rates, and flow velocity (Lai et al., 2018; Farin et al., 2019). Navratil et al. (2013) showed that the seismic signal envelope of debris flow surges is conserved as the surge travels along the torrent. Surge waves have larger peak flow heights and are faster than the bulk flow, leading to higher particle impact rates, larger particle momentum, and increased basal forces compared to the bulk flow (Razis et al., 2014; McArdell, 2016). Therefore, in theory, dense near-torrent seismic measurements should be able to resolve passing surge waves as elevated high-frequency (1–100 Hz) signals, in contrast to seismic stations further away from the torrent that record the integrated seismic signal (Fig. 1b) of the entire debris flow (Tsai et al., 2012; Lai et al., 2018).

In this study, we used distributed near-torrent seismic measurements at the Illgraben debris flow observatory maintained by the Swiss Federal Institute for Forest, Snow and Landscape Research WSL to analyze the spatiotemporal evolution of debris flow surges from

the catchment into the valley. A comparative analysis of near-torrent seismic observations with flow height measurements and video footage enables us to identify different flow regions and surge waves in the seismic data, to track their seismic signatures along the torrent, and to estimate their propagation velocities. Furthermore, the distributed observation of debris flows helps us to capture the process of surge wave formation, which to the best of our knowledge was never done before with such high spatial resolution. Finally, we characterize erosion-deposition waves at Illgraben using flow height measurements. We address the following questions:

1. Can distributed near-torrent seismic sensing of debris flows reveal flow dynamical processes such as surge propagation and surge wave formation and therefore bridge the gaps between small-scale laboratory experiments, point measurements in the field and numerical simulations?
2. Can the results be used to resolve surge wave formation within debris flows, and can these findings validate existing laboratory-scale experiments and theoretical models of surge waves?

## 2. Debris flow monitoring at the Illgraben torrent system

The Illgraben torrent system is located in the Rhône Valley in the Swiss Alps (Fig. 2a). Illgraben is one of Europe's most active debris-flow catchments. Draining a 9 $km^2$ catchment system, Illgraben produces on average 5 debris flows per year, which reach the channel outlet at the Rhône River (Badoux et al., 2009). The steep (on average 40%) unstable slopes in Illgraben's upper catchment consist of highly fractured Triassic schists, dolobreccias and quartzites (Schlunegger et al., 2009) supplying sediment to the uppermost channel reaches. From there, material is episodically mobilized into debris flows during intense summer precipitation events or snow melt in spring. The torrent stretches from 2717 m above sea level (a.s.l.) to its outlet at 850 m a.s.l. from where it flows another 2 km over its Holocene debris fan and merges with the Rhône River at 630 m a.s.l. close to the municipalities of Susten and Leuk (Valais). A 47-m-tall check dam (CD1) was built in the 1970s to stabilize the catchment after a rock avalanche followed by a large debris flow that destroyed a cantonal road bridge near Leuk in 1961 (Missbauer, 1971). Subsequently, 29 check dams (3–5 m high) were built along the Illgraben torrent to minimize channel erosion and stabilize the channel bed (McArdell and Sartori, 2020). Images of selected check dams are shown in the Supplementary Information S2.

A debris-flow observatory maintained by WSL was installed on the fan in the year 2000 and has been continuously upgraded since then (Hürlimann et al., 2003; McArdell et al., 2007). It now contains automatic cameras, geophone plates installed on check dams for front velocity estimation (Belli et al., 2022), radar and laser-based flow stage sensors (Badoux et al., 2009), 3D-LiDAR scanners (Aaron et al., 2023; Spielmann and Aaron, 2024), an in-torrent force plate (McArdell, 2016; Zhang et al., 2021a) as well as rain gauges in the catchment and on the fan (Hirschberg et al., 2021). In addition, a semi-permanent seismometer network has been deployed in the surrounding area of the Illgraben catchment (Marchetti et al., 2019; Chmiel et al., 2021; Belli et al., 2022, 2025), to monitor landslide and debris flow activity.

Surge waves are regularly observed at Illgraben (e.g. McArdell, 2016) as debris flows leave the catchment and cross the 2-km long fan. The steady uniform flow disintegrates into a sequence of up to meter-high surge waves forming a quasi-periodic wave train (Aaron et al., 2025).

## 3. Experimental set-up and methods

### 3.1. Nodal-array and seismometers

In this study we deployed 33 SmartSolo (IGU-16HR 3C) seismic nodes along the Illgraben torrent (Fig. 2), with 5 Hz natural frequency and flat response up to the Nyquist frequency (125 Hz). Node spacing and sensor-torrent distances were approximately 50–70 m and 5–40 m, respectively (Supplementary Information S3). In total, the nodal array covers a torrent section of about 2200 m from the fan apex to the confluence with the Rhône River (Fig. 2b). The nodal-array was recording for 38 days starting on 24 May 2024.

Additional seismic data were collected by two solar-powered Lennartz (LE-3Dlite MkIII, 3C) seismometers (ILL12, ILL22) installed in the Illgraben catchment (Fig. 2a) with 1 Hz natural frequency and flat response up to the Nyquist frequency (50 Hz). Station ILL12 is located 85 m from the torrent near Check Dam 10 (CD10) and station ILL22 is located 15 m from the torrent close to Check Dam 1 (CD1). The combined node/seismometer network covers a 4-km torrent section and resolves the propagation of debris flow surges from the catchment into the valley. In Fig. 3 the vertical-component seismograms of all 35 stations are shown with respect to their torrent position for a debris flow recorded on 15 June 2024 at Illgraben. Two debris flow surges are recognizable as high-amplitude regions that migrate down the torrent. Within the main surge, multiple sub-surges are visible as secondary amplitude peaks.

#### 3.1.1. Seismic data processing

The raw, vertical-component, data of all 35 seismic stations are first corrected for the instrument response to convert digital counts to ground velocity (Fig. 3). In a second step, the Power Spectral Density (PSD) is computed for each station in 1-second windows with 50% overlap between the instrument-specific lower corner frequency and the Nyquist frequency (SmartSolo: 5–125 Hz, Lennartz: 1–50 Hz). We calculate the mean PSD within a frequency bin of 30–90 Hz for the SmartSolo nodes and 30–50 Hz for the two Lennartz seismometers. We exclude frequencies below 30 Hz in order to suppress seismic noise generated at fixed positions along the torrent, in particular flow turbulence below check dams (Marchetti et al., 2019), which at Illgraben is typically observed within a frequency band of 1–10 Hz (Belli et al., 2025). This workflow is applied to all 35 seismic stations, and in the last processing step the mean PSD of all stations is resampled onto a regular 5-m grid showing the spatiotemporal evolution of the measured mean PSD of the entire debris flow event. In the Supplementary Information S2, we show low-frequency seismic signals induced by Check Dam 1 that we detect kilometers away in the valley.

#### 3.1.2. Surge velocity measurement through seismic signal tracking

The main debris flow fronts, subsequent surges, and surge waves generate high-frequency ground vibrations (McArdell, 2016; Farin et al., 2019; Coviello et al., 2019), whose signal envelope is stable as measured by seismic stations along the torrent (Navratil et al., 2013). We identify surge fronts and surge waves on video footage and flow height measurements and track the associated seismic signal patterns along the torrent. The velocities of the debris flow front and subsequent surge waves are estimated as the ratio of the distance between seismic stations and the corresponding time delay between the signal patterns.

### 3.2. Video cameras, radar and LiDAR sensors

We use flow depth data and webcam videos from sensors installed on channel crossing cables at CD27 (Fig. 4) and CD28. Data recording is triggered by threshold-based alarms using separate geophones mounted on check dams (Badoux et al., 2009). Radar-based distance sensors (VEGA, model VEGAPULS C22) are used to obtain hydrographs of debris flows. They have a sampling rate of 1 Hz and a factory precision of ±2 mm (Vega, 2025). The data are stored with a precision of ±1 cm to account for elevation variations within the radar footprint. Flow height is deduced from the initial elevation before debris flow events and does not include possible erosion and deposition that occurred relative to the pre-event surface.

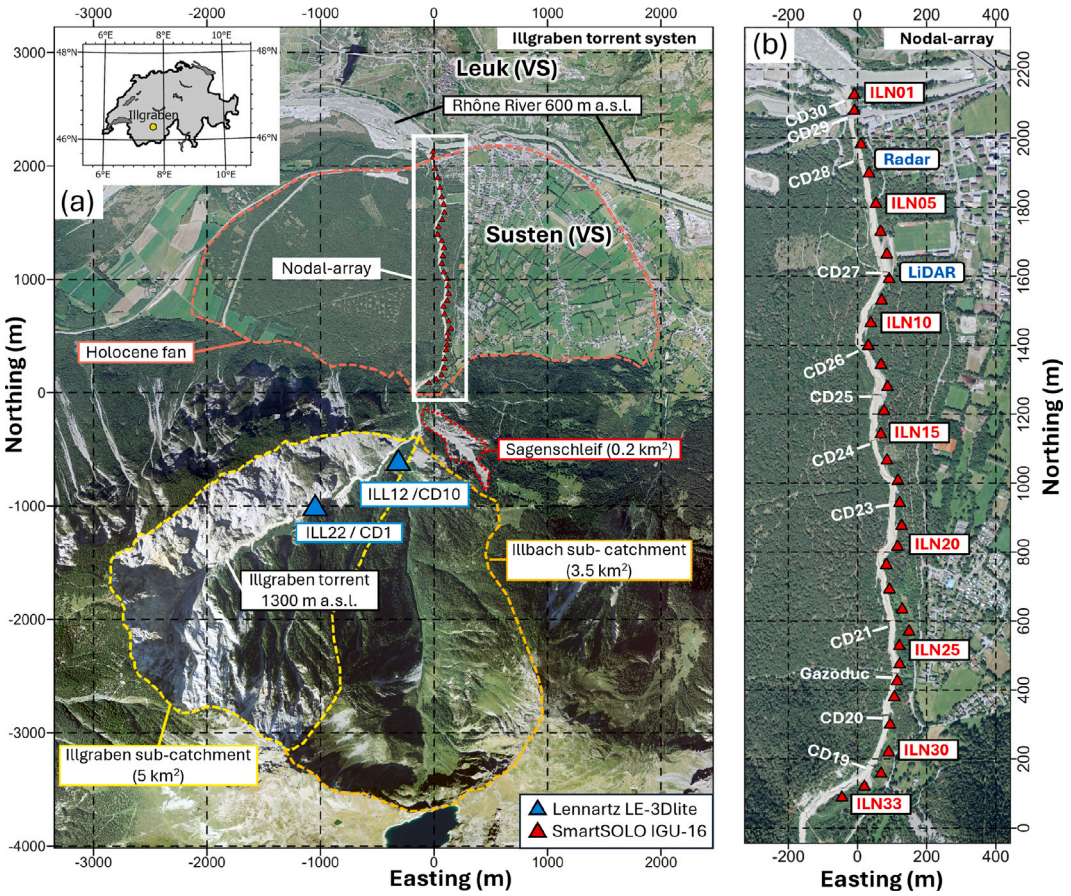


**Fig. 2.** Illgraben torrent system in the Rhône valley in the Swiss Alps. Debris flows mobilize in the Illgraben sub-catchment, flow along the Illgraben torrent and merge with the Rhône River in the valley. (a) Overview map of the Illgraben investigation site. Two seismometers are installed in the Illgraben catchment. (b) Closeup section of the Illgraben torrent crossing the 2200 m channel on the Illgraben fan. Check dams (CD) built along the torrent are indicated. 33 SmartSolo seismic nodes were installed along the 2-km torrent section. LiDAR and radar sensors were installed at CD27 and CD28 respectively (Orthophotos: Swiss Federal Office of Topography swisstopo).

In addition, a midrange, multibeam high-resolution 3D LiDAR scanner (Ouster OS1-128) is installed at CD27 and used to derive additional debris flow hydrographs with a sampling rate of 10 Hz (e.g. Spielmann and Aaron, 2024). The precision of the sensor is ±0.5 cm for ranges of 1 m–20 m (Ouster, 2025). The LiDAR scanner covers a flow section between ca. 30 m upstream and downstream of CD27, but for the purpose of this work, we derive the average flow height in a 2 m × 2 m wide box in the middle of the channel 10 m upstream of the sensor. Details of the derivation of flow height hydrographs from the LiDAR scanner are described in Aaron et al. (2023) and Spielmann et al. (2025).

### 3.3. Flow height and surge front velocity measurements

Similar to Schöffl et al. (2023), we calculate the amplitude $A$ of each erosion-deposition wave as the difference between the peak flow height $h$ and the thickness of the stationary erodible layer $h_{stop}$ downstream of each erosion-deposition wave with $A = h - h_{stop}$ and the surge period $T$ as the time between subsequent surge wave passages using flow height data recorded at CD27 and CD28 as shown in Fig. 4c. Continuous flow height recordings can be used to derive the travel times and velocities of surges (Zhang et al., 2021a) and surge waves between two sensors. We use the LiDAR sensor installed at CD27 and the radar sensor located 350 m downstream at CD28 to pick travel times from the flow height hydrographs (Supplementary Information S4) and derive front velocities of erosion-deposition waves ($v_s$). Moreover, we use the following equation derived by Razis et al. (2014) to estimate front velocities of erosion-deposition waves:

$$v_S = \sqrt{\frac{1}{2} g \cos\theta \, (2h_{stop} + A)(h_{stop} + A)/h_{stop}} \quad (1)$$

Here, $g$ denotes the acceleration due to gravity (9.81 m/s$^2$) and $\theta$ is the local slope angle (4.6°) at CD27. This approach, previously applied by Chen et al. (2024) for erosion-deposition waves observed at Jiangjia Ravine (Yunnan Province, China) assumes non-viscous behavior at the steep front of erosion-deposition waves caused by high shear rates. Furthermore, we assume that erosion-deposition waves at Illgraben erode the entire static layer, which we consider a reasonable assumption near check dams at Illgraben where $A$ and $h_{stop}$ are measured.

## 4. Observations and results

During the 2024 debris flow season, 36 torrential events were registered at Illgraben. Smaller debris flows with less than 1 m flow height (at CD27) and debris floods were observed in March and April. From May to July, several large debris flows were recorded with up to 2.5 m flow height, showing complex flow dynamics, including surge waves and precursory debris floods. Smaller events and debris floods were observed between August and October. We were able to record nine debris flows with the nodal array between 24 May 2024 and 1 July 2024, ranging from slow granular flows to fast-flowing debris floods and surge wave-driven pulsating flows. During the recording period, 93 mm of rain were recorded at the measurement station at CD1 in the

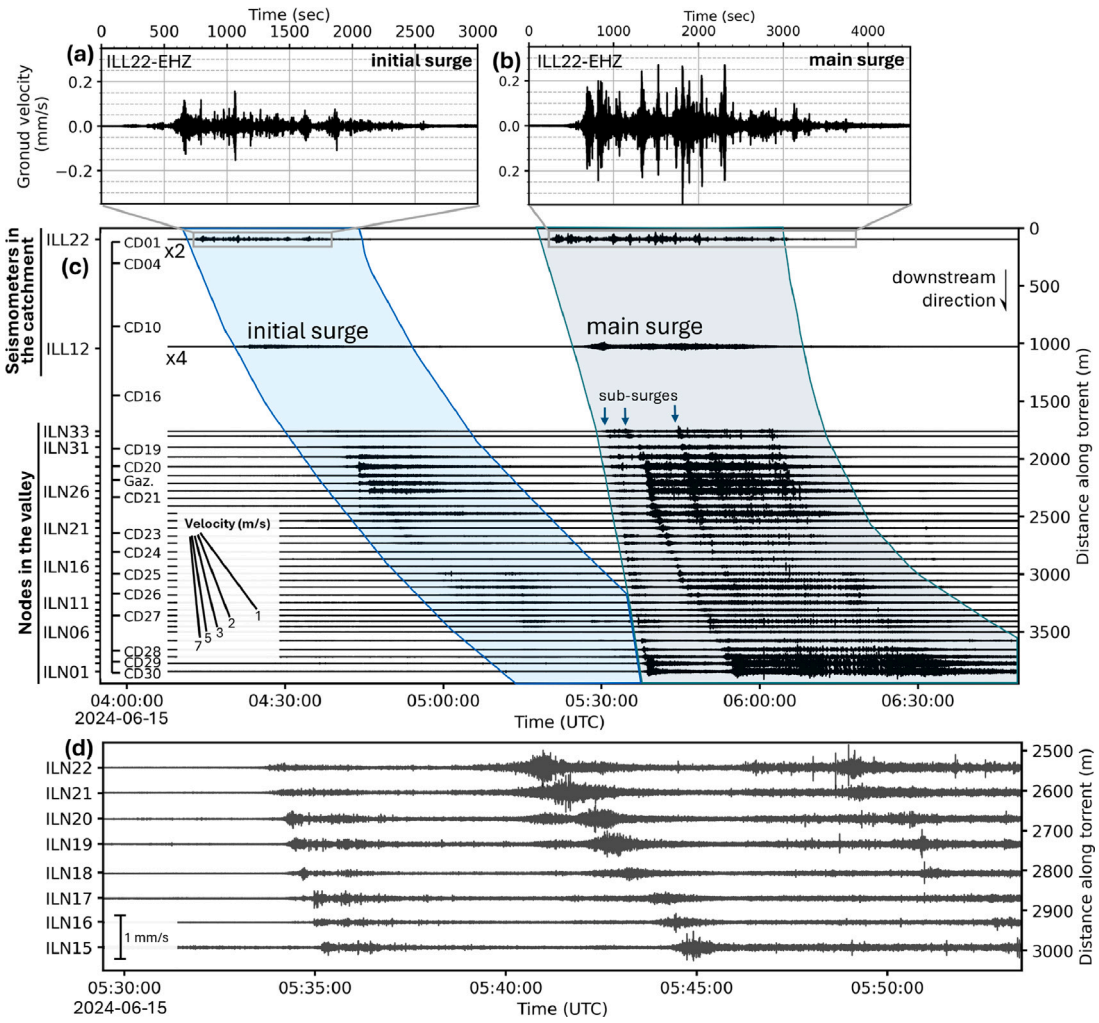


**Fig. 3.** Vertical-component seismograms of 35 seismic stations along the Illgraben torrent starting upstream at CD1 (ILL22) in the catchment. ILL22 and ILL12 are Lennartz seismometers and ILN01-33 are SmartSolo IGU16 seismic nodes. Shown is the debris flow recorded on 15 June 2024. Two consecutive surges occurred 1-hour apart and were observed on the nodal-array during the outflow phase. (d) Zoomed-in section of (c) showing two debris flow sub-surges flowing along the torrent. During their propagation, the surge exhibit stable signal shapes.

catchment. In Fig. 5 we give a visual overview of the recording time period.

In this study, we focus on three events recorded on 15 June 2024 (04:20:00 UTC, local time -2) and 21 June 2024 (07:10:00 and 12:10:00 UTC), shown in Fig. 5. The events were selected for two reasons: (1) They showed flow dynamical complexity, surging behavior, and developed large-scale surge waves and (2) all three events occurred during daylight hours, which allowed for analysis of video data. For simplicity, we use the abbreviations Event 1 (15 June 2024), Event 2 (21 June 2024, morning), and Event 3 (21 June 2024, noon) for these three events. Timelapse videos (10x speed) captured from Camera 2 at CD27 can be accessed via direct links in Section 7.

On 15 June 2024 04:51:00 (UTC) the nodal array recorded a debris-flow event lasting 90-minutes (Event 1). In Fig. 6 webcam frames taken at CD27 (Camera 2) are shown and in Video V1 (see Section 7) a timelapse movie of the entire event is presented, which was used to identify multiple event phases. The event starts with a precursory flood of muddy water (04:52:00 UTC at CD27) followed by an initial debris flow with granular composition (Fig. 6b). This precursory event was followed by a 60-minute long main surge, starting at 05:36:45 UTC with a debris flood (Fig. 6c), which was followed by a bouldery debris-flow surge (Fig. 6d). Between 05:50:00 and 06:20:00 UTC the continuous flow transformed into a sequence of surge waves, forming a pulsating flow, as observations at CD27 (Video V1, after 05:00 min) show. During the pulsating flow phase, meter-high erosion-deposition waves are observed traveling over a static erodible layer deposited by the previous wave (Fig. 6f) similar to what Schöffl et al. (2023) observed at the Gadria creek in Italy. At CD27 we record flow stopping regions that remained stationary for up to 60 s before the arrival of the next wave. In the last phase of the debris flow, the flow tail quickly erodes away the previously deposited static layer over a period of about five minutes after which no further erosion-deposition waves are observed.

### 4.1. Seismic record of debris flow (Event 1)

In Fig. 7 we show a comparative analysis between near-torrent seismic recordings of nodal station ILN08 (see map Fig. 2b) and flow height measurements using a LiDAR scanner at the same location (CD27) for Event 1. The event visually started as a fine sediment-laden water flow, recognizable as a broad-band seismic signal (Fig. 7b) followed by two flood peaks with up to 8 cm flow height 600 s later (Fig. 7c).

Comparison of the seismic data with webcam footage and flow height measurements allows us to identify (1) the precursory flood, (2) the initial surge, (3) the debris flood, (4) the main bouldery surge, (5) the pulsating flow with surge waves, and (6) the muddy flow tail (Fig. 7b). The strongest seismic signals are registered during the passage

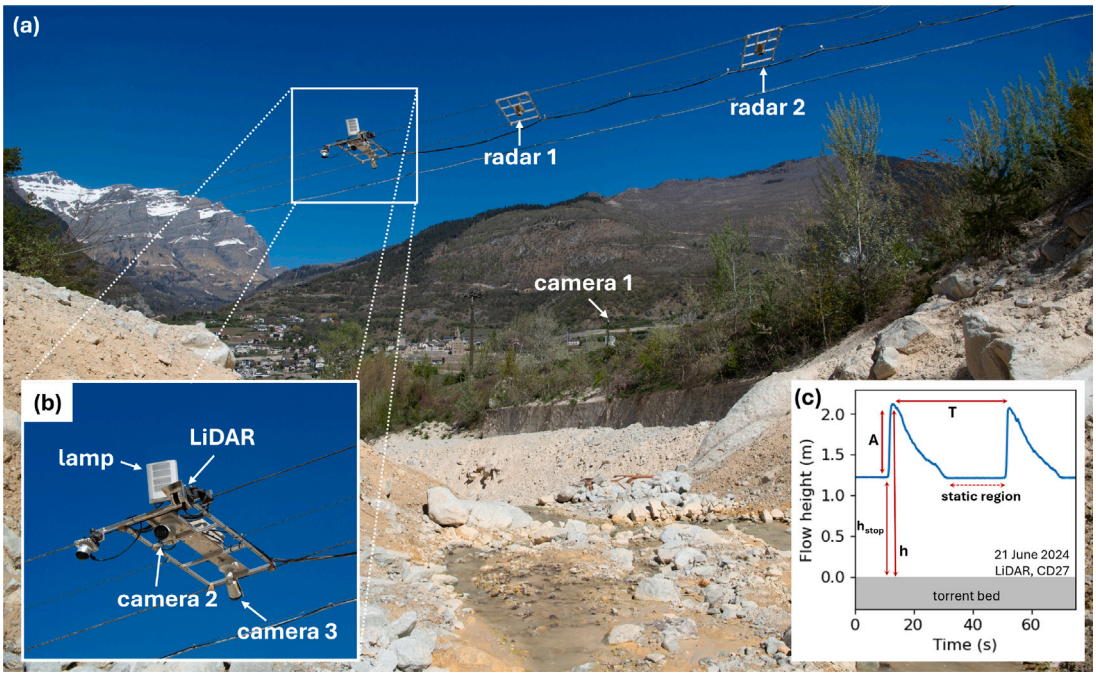


**Fig. 4.** (a) Overview of the Illgraben debris-flow monitoring station installed at CD27. Sensors are suspended about 4 m above the channel bed and are triggered by a geophone installed on CD25, 380 m upstream. (b) The LiDAR sensor used here is an Ouster OS1-128 with a frame rate of 10 Hz. (c) LiDAR based flow height hydrograph of two consecutive erosion-deposition waves.

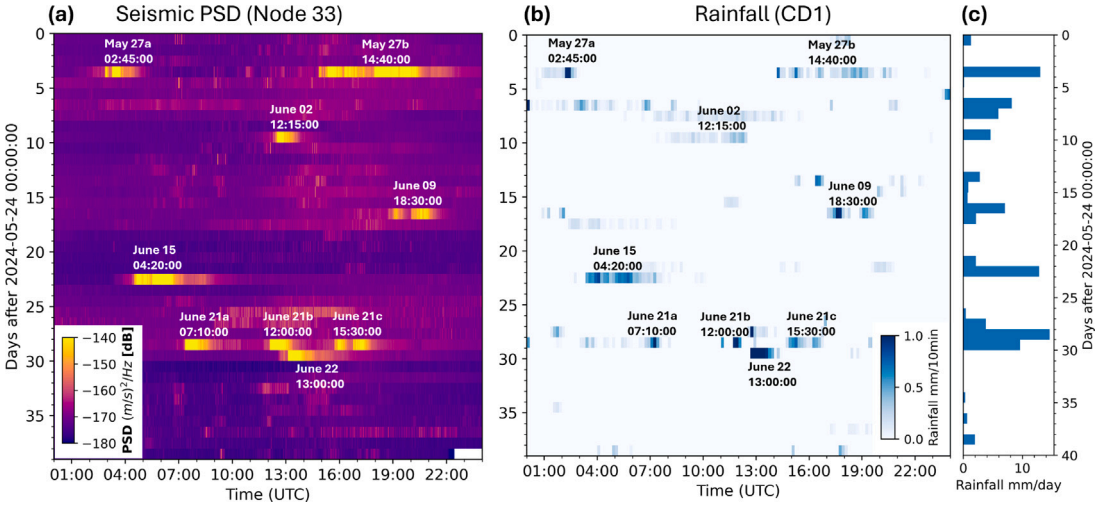


**Fig. 5.** Evolution of (a) continuous mean seismic power spectral density (5–125 Hz, 1-sec window, 50% overlap) recorded from seismic node ILN33, located at the fan apex, between 24 May 2024 and 1 July 2024, (b) rainfall measured near Check Dam 1 in the catchment and (c) daily rainfall. Nine debris flows are visible as hour-long high-amplitude seismic signals.

of the debris flood and the bouldery debris flow surge where vertical ground velocities reach 1 mm/s and peak seismic power levels are 50 dB above ambient.

After the passage of the bouldery surge at CD27, a sequence of meter-high surge waves is recognizable in the seismic data (Fig. 7d) as well as on the hydrograph (Fig. 7e). Based on video material (Video V1, between 04:50 and 05:30 min) and flow height data (Fig. 7e), the flow remains fully mobilized for the first 13 surge waves (RW1-13 in Fig. 7), which we therefore classify as roll waves. Starting at 4750 s in Fig. 7d a meter-thick erodible layer forms as the bulk flow comes to rest and only periodically remobilizes during the passage of surge waves (Video V1, after 05:30 min). Stopping regions are further visible as flat hydrograph response ($h_{stop}$) in Fig. 7e. During stopping regions between waves, we find a decrease in seismic power of up to 30 dB, which is in contrast with roll waves where we only observe seismic power fluctuations of around 10 dB. We classify these waves (EDW1-18 in Fig. 7) as erosion-deposition waves (Edwards and Gray, 2015; Schöffl et al., 2023) with a flow height of up to 2 m that travel over an erodible layer with a thickness of 1 m. We note that for EDW1-3 the flow does not fully stop between the waves and we suspect that EDW1-3 are in the process of merging.

Toward the end of the initial surge, the video material (Video V1, after 02:20 min) shows that flow velocities drastically decrease. The flow came to rest multiple times subsequently and was remobilized through subsequent upstream inflow of new material after tens of seconds of standstill. This process is visible on the seismic data as a

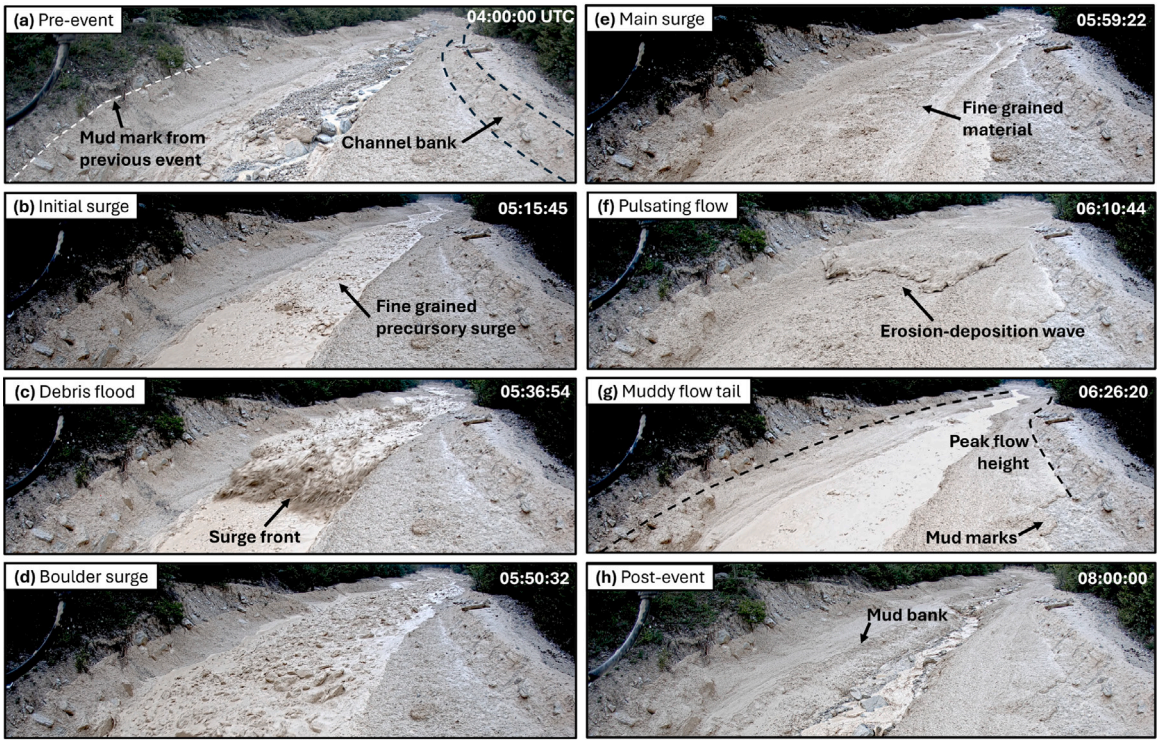


**Fig. 6.** Video stills from Video V1 of the arrival of different flow fronts of the 15 June 2024 debris flow at Illgraben captured with a webcam installed at CD27, pointing upstream. Video is accessible in Section 7.

drop in seismic power during static conditions followed by a sudden increase during re-mobilizations (s3, s4 in Fig. 7b).

### 4.2. Distributed measurement of debris flows

#### 4.2.1. Event 1: 15 June 2024

Fig. 8 combines the seismic data of all 35 stations (ILL22, ILL12 and ILN01-33) into a single spatiotemporal representation of the debris flow as described in Section 3.1.1. The recorded amplitudes of different stations vary substantially due to site response and path effects. Differences in sensor-torrent distance greatly affect the recorded signal strength. The mean sensor-torrent distance is 12 m for stations ILN01-33. Stations ILN23 - 25 are installed further away from the torrent (28, 42 and 20 m) due to topographic constraints, and attenuation results in much weaker seismic signals (Fig. 8b). In contrast, the nearby nodal station S26 is located only meters downstream of the check dam at the Gazoduc station and therefore records elevated seismic energy (Fig. 8b). Starting at 03:20:00 UTC the nodal array records high frequency (> 60 Hz), rain-induced seismic noise (Hua et al., 2023) indicated in Fig. 8a. Tree cover affects the rain signal, leading to different amplitudes along the channel (Supplementary Information, S1).

The distributed seismic data allow us to track the amplitude signatures observed on the single station (ILN08 at CD27) in Fig. 7 along the torrent and therefore to map debris-flow evolution on kilometer scales in time and space. The seismic data reveal two consecutive debris flows, triggered one hour apart in the Illgraben catchment (initial surge, main surge in Fig. 8b) that start merging in the downstream part of the channel as the fast-moving debris flood front (5 m/s) of the main surge caught up to the tail of the slower-moving initial surge (1–2 m/s) visible as the overlap of their seismic signatures (Fig. 8b). As the initial surge reaches the nodal array (ILN01-33) the seismic signals reveal two flow regions. (1) A precursory flood and (2) the remnant of the initial surge observed at CD1 (s0 in Fig. 8b). Below CD25 the seismic signal of the initial surge (s0) splits into two sub-signals s1 and s2 (black box in Fig. 8b). Based on video material from CD27 and by comparison with Fig. 7b we identify s1 as flood peaks and s2 as the remainder of the initial surge (s0) observed upstream of CD24. Therefore, seismic data suggest that downstream of CD24, the flood peaks (s1) bifurcated from the initial surge (s0), while s2 represents the remainder of the initial surge (s0). Furthermore, the distributed data illuminate the flow dynamics within the flow tail of the initial surge. We find that regions of stopping and remobilized flow (s3 and s4), previously recognized in point measurements at CD27 (Fig. 7b), propagate downstream with about 3 m/s.

The main surge starts with a fast-moving debris flood (5 m/s front velocity), followed by multiple, slower-moving bouldery surges (B1, B2 in Fig. 8c). For bouldery surge B1 in Fig. 8c, we find that approximately at check dam CD25, the front suddenly slows down before accelerating again to about 2 m/s after a few minutes.

In the later part of the main surge we observe the disintegration of the continuous flow into a series of quasi-periodic erosion-deposition waves (Fig. 8c). Stripes of high seismic power in Fig. 8c mark the propagating waves, whereas dark bands, with lower seismic power, interlacing the waves, mark the flow stopping regions, as previously seen in the seismic record of nodal station ILN08 in Fig. 7. We find that erosion-deposition waves have constant propagating velocities between 5–6 m/s and, therefore, are substantially faster than the bouldery surges (2–3 m/s). Furthermore, the seismic data reveal that erosion-deposition waves develop (“spawn”) consecutively out of a flow section of only a few 100 m length within the flow tail of the debris flow. This spawning zone itself moves downstream with about 1 m/s. The downstream propagation of the spawning zone has the effect that for an observer at a fixed location along the torrent, subsequently arriving waves are sorted according to their travel distance: earlier arriving waves have their origin further upstream than later ones. Furthermore, we observe erosion-deposition waves that cross bouldery surge B1 and transform into roll waves, without stopping regions, as previously seen in Fig. 7d.

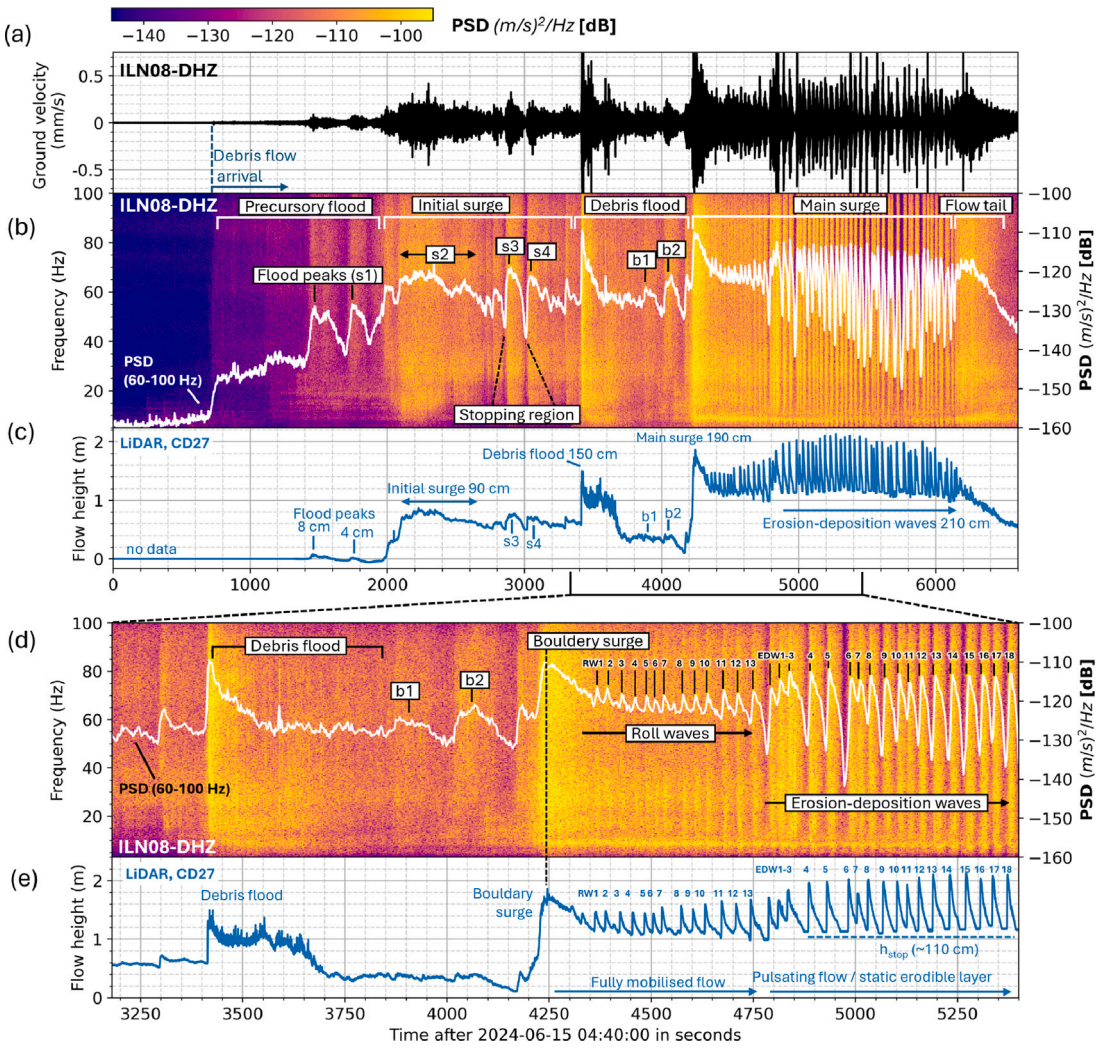


**Fig. 7.** Near-torrent seismic observation of debris flow recorded on 15 June 2024 at Illgraben. (a) Vertical-component seismogram of debris flow recorded with seismic node ILN08 near CD27. (b) Vertical-component spectrogram of Event 1. (c) LiDAR-based flow height measurement obtained at CD27, close to the seismic node. (d-e) Close-up of the main surge. Thirteen roll waves (RW1-13) are followed by 18 erosion deposition waves (EDW1-18). Flow stopping regions between erosion-deposition waves are clearly visible as dark, low-amplitude bands in the seismic data as well as flat hydrograph sections in (e).

#### 4.2.2. Event 2: 21 June 2024 (morning)

The surge behavior of Event 2 is different, because no precursory surges or debris floods were recorded prior to the arrival of the main surge (Fig. 9). Instead, Event 2 abruptly starts with a bouldery front. The distributed seismic measurements allow us to track the front along the 2-km torrent section and determine the front velocity (Fig. 9d). Between CD1 and CD26 we observe a constant front velocity of 2.9 m/s. Downstream of CD26 the front slows down and we estimate a front velocity of 1.4 m/s.

In the later stage of the debris flow, the continuous flow disintegrates into a series of erosion-deposition waves (Video V2 in Section 7) that last for 60 min in the downstream channel section, recognizable as diagonal high-amplitude bands in the seismic data (Fig. 9d). Similar to Event 1 surge waves spawn out of the debris flow tail and travel with constant velocity. During the initial phase of the flow, when the front is traveling along the nodal array, we observe fast moving erosion-deposition waves (5–6 m/s) catching up and merging with the slow moving front (1–3 m/s). We do not observe surge waves traversing the front.

#### 4.2.3. Event 3: 21 June 2024 (noon)

Only five hours after Event 2 has been registered and 2.5 mm of additional rainfall had been measured at CD1 a second debris flow was triggered. The debris flow started with a debris flood (Video V4, Section 7) followed by a bouldery surge visible as a downward propagating band of seismic energy (Fig. 10). Event 3 also produced surge waves visible in video materials (Video V3, Section 7). Compared to Event 1 and Event 2 we observe a sequence of roll waves instead of erosion-deposition waves. The seismic signature of roll waves is less prominent than the signature of erosion-deposition waves due to the lack of a flow stopping zone. We can nevertheless identify roll waves spawning out of the rearward part of the debris flow, but as a result of weaker surge wave signals, the spawning zone is less prominent compared to Events 1 and 2. In the later stage of the event, after 12:40:00 UTC, downstream of CD27, the seismic data reveal the formation of erosion-deposition waves. Video material recorded at CD28, 300 m downstream of CD27, shows how the bulk flow drastically slows down after 12:35:00 (Video V4, Section 7) and subsequent surge waves develop stopping regions within the wave troughs after 12:40:00 UTC turning roll waves into erosion-deposition waves.

### 4.3. Observations of surge wave formation

All three events presented in Section 4.2 exhibit a surge wave spawning zone that slowly migrates downstream. In Fig. 11 we show a comparative analysis of the spawning zone based on seismic data

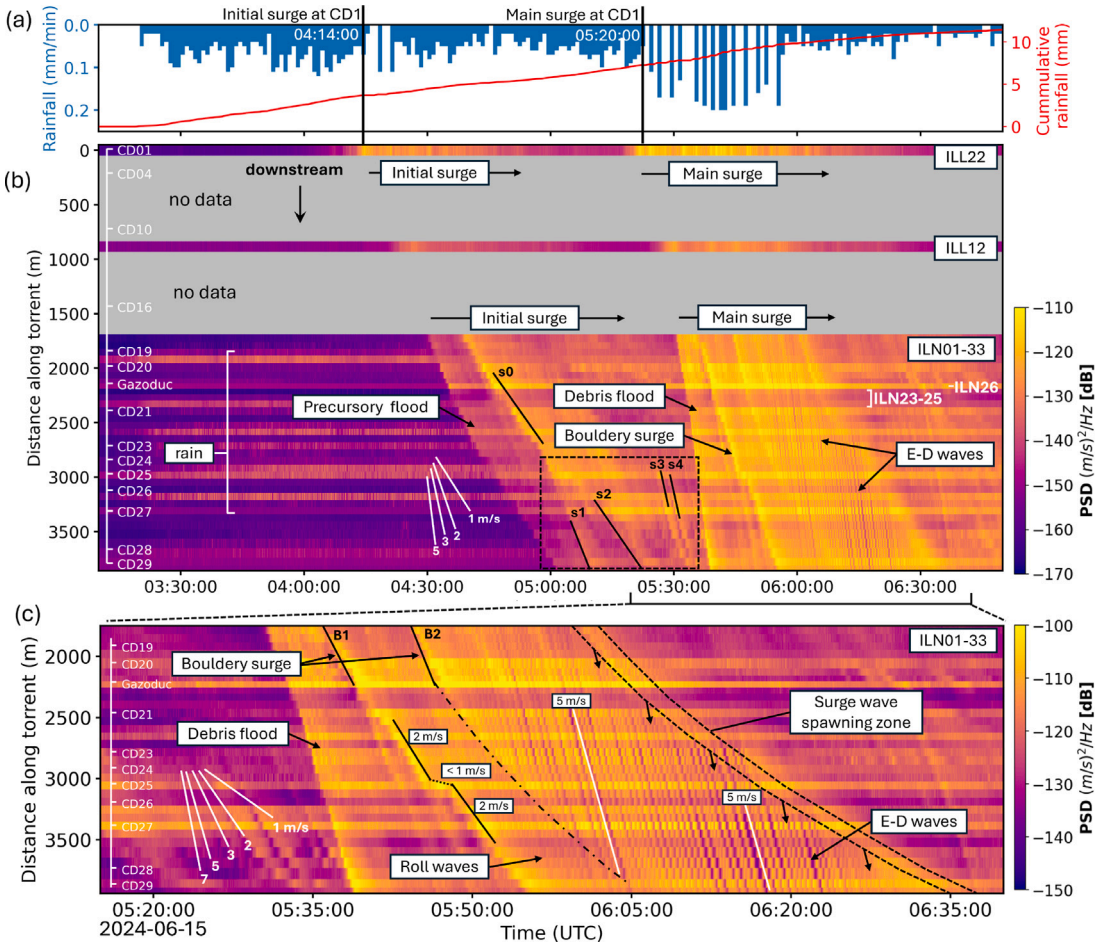


**Fig. 8.** Event 1: Time-distance visualization of debris flow recorded on 15 June 2024 at Illgraben. (a) Rainfall measured at CD1 in the catchment. (b) Spatiotemporal evolution of mean power spectral density (PSD) for all 35 seismic stations. Initial surge and main surge initiate 60 min apart in the catchment, flow along the torrent and start merging downstream of check dam CD25. (c) Close up of (b) highlighting the formation of erosion-deposition waves (E-D waves) out of the flow tail.

(seismic node ILN08) and LiDAR flow height measurements at CD27. We observe a sudden onset of surge wave formation in all three events. In Event 1 erosion-deposition waves emerge out of a relatively thick flow with a flow height of up to 1 meter (Fig. 11a). Within hundreds of meters of flow distance, meter-scale erosion-deposition waves form to produce a regular wave train with flow stopping regions between waves. In Event 2 and 3 (Fig. 11b,c) the flow height inside the spawning zone is smaller (< 0.5 m) and we observe the formation of irregularly shaped roll waves with smaller wave heights than Event 1. Moreover, in Event 2 we observe the transition from regular roll waves into larger erosion-deposition waves. Furthermore, flow height data reveal small-scale flow undulations (< 0.2 m) upstream of the spawning zone within the flow tail that travel faster than the bulk flow as video material shows (Video V1, after 08:00 min).

### 4.4. Characterization of erosion-deposition waves at Illgraben

We estimate key characteristics of erosion-deposition waves observed in Event 1 (analyzed waves, $N = 15$) and Event 2 ($N = 35$). As Event 3 does not produce clear erosion-deposition waves with stopping regions at check dam CD27 we exclude this event from the subsequent analysis. Flow heights of erosion-deposition waves and surge-front velocities are calculated as described in Section 3.3. We find increasing surge front speeds ($v_s$) with increasing wave height ($A$) and increasing stopping height ($h_{stop}$) (Fig. 12c-d). Furthermore, we find a correlation between wave height ($A$) and stopping height ($h_{stop}$) (Fig. 12e), which indicates that wave height is controlled by the thickness of the erodible layer. In Event 2 we find decreasing stopping heights and erosion-deposition wave velocities over time (Fig. 12f,g). Using Eq. (1) we estimate erosion-deposition wave front velocities and compare them to hydrograph-derived front velocities, as described in Section 3.3. We find good agreement between measured and calculated velocities with an average velocity error of about 19%. Furthermore, we estimate the surge front Froude number of erosion-deposition waves using $Fr = v_s/\sqrt{g\,h\,\cos\theta}$ and find median Froude numbers of 1.2–1.25 for both events. Flow height data of both events further show that the wave height ($A$) of erosion-deposition waves is slightly smaller than the thickness of the erodible layer through which the waves propagate.

## 5. Discussion

### 5.1. Formation of surge waves

Surging behavior of debris flows has been explained by different mechanisms: at the catchment level, sediment capacitors (Kean et al., 2013) or the blocking effect of landslide dams (Guo et al., 2020) have been suggested. At Illgraben, surge wave formation typically starts much later during the outflow into the valley, as seen in our measurements (Section 4.2) as well as in recent studies by Aaron et al. (2025) and Spielmann et al. (2025). Therefore, such processes, linked to debris flow mobilization within the catchment, are unable to explain the observed surge wave trains, as their formation takes place much

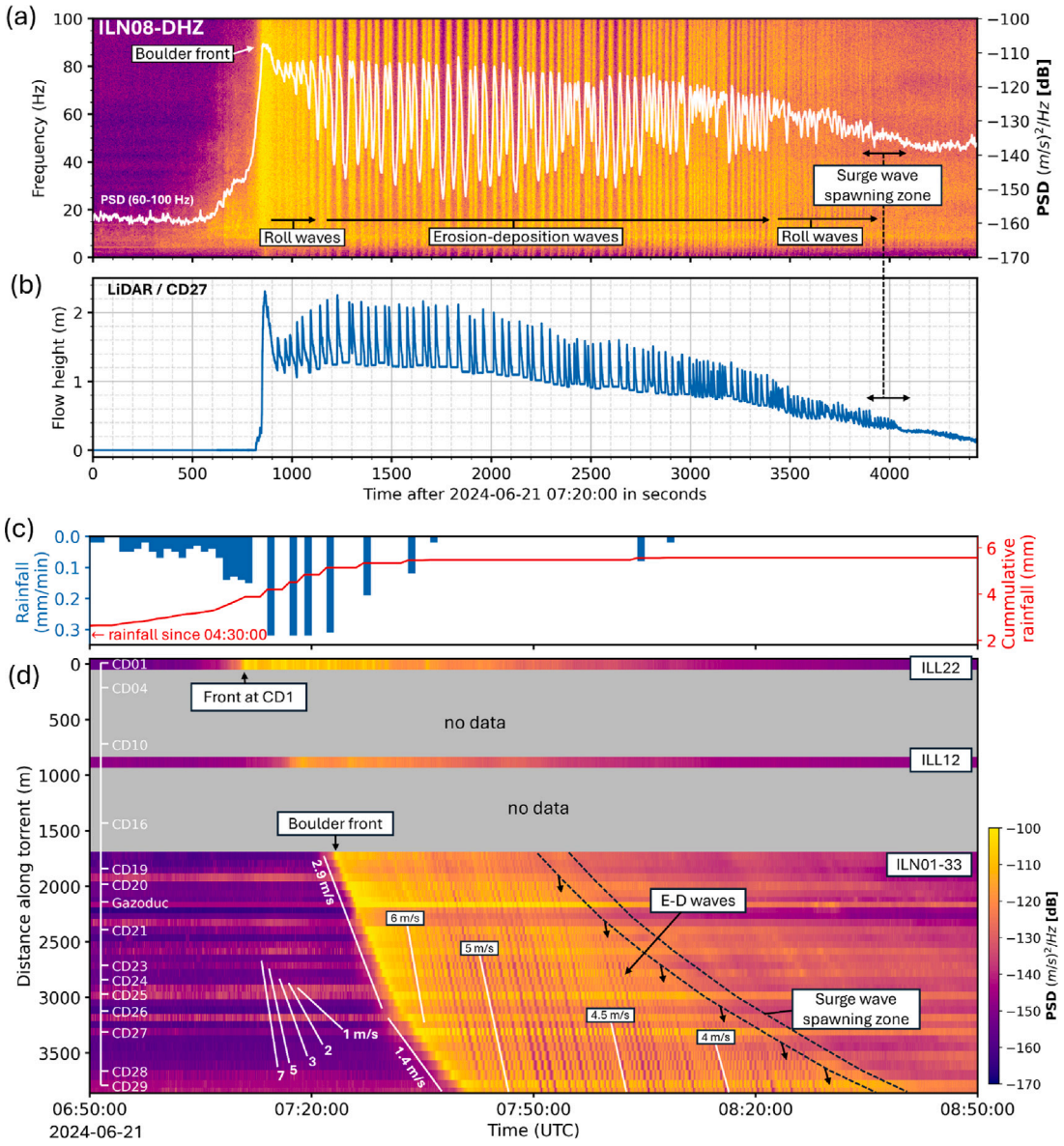


**Fig. 9.** Event 2: (a) Vertical-component spectrogram of station ILN08, located close to CD27. White line represents the mean power spectral density (PSD) between 60–100 Hz. (b) LiDAR-based flow height measurement at CD27. (c) Rainfall measured at CD1 in the catchment. (d) Spatiotemporal evolution of mean power spectral density (PSD) for all 35 seismic stations. Erosion-deposition waves (E-D waves) spawn in the flow tail and propagate along the Illgraben torrent with constant velocity.

later, during runout, when debris flows have already left the catchment and propagate on the fan (Spielmann et al., 2025).

During the runout phase, surge formation has been attributed to grain-size segregation (Johnson et al., 2012), basal entrainment (Iverson, 2012), and flow instabilities (Trowbridge, 1987). Grain-size segregation explains surge formation with the segregation of large particles to the flow surface, where the velocity is greatest, resulting in their preferential transport to the flow front. Such processes can contribute to the formation of bouldery surge fronts, which are frequently observed at Illgraben (McArdell, 2016). However, surge wave trains do not show grain size segregation or boulder accumulation at the wave crest (Spielmann et al., 2025), and therefore, grain-size segregation is unlikely to play a major role in surge wave formation at Illgraben. Finally, surge waves may result from flow instabilities. (1) Free-surface instabilities (Trowbridge, 1987; Forterre and Pouliquen, 2003; Forterre, 2006; Gray and Edwards, 2014; Edwards and Gray, 2015; Viroulet et al., 2018; Aaron et al., 2025) are driven by gravity and the resultant frictional feedback of the flowing material, which leads to the amplification of small flow height undulations into large-scale surge waves. These are closely related to classical roll waves, observed in open water channels (e.g., Jeffreys, 1925; Dressler, 1949). (2) Basal entrainment leading to instabilities occurring at the interface between the flowing granular mass and an initially static erodible bed (Mangeney et al., 2010; Iverson, 2012; Farin et al., 2014; Edwards et al., 2019) which can lead to wave-like granular avalanches (e.g., Edwards et al., 2017). In the following, we discuss evidence that flow instabilities are responsible for surge wave formation at Illgraben.

Our distributed measurements of debris flows, presented in Section 4.2, capture dynamic effects at the highest spatial resolution ever recorded at Illgraben. They provide direct evidence regarding where surge waves develop (spawn) and how they evolve in time and space. The spontaneous formation of surge waves takes place only within the muddy flow tail of the observed debris flows, up to kilometers upstream of the front (Figs. 8–10). We observe a spatio-temporal pattern of wave formation, as the spawning zone slowly migrates along the channel in

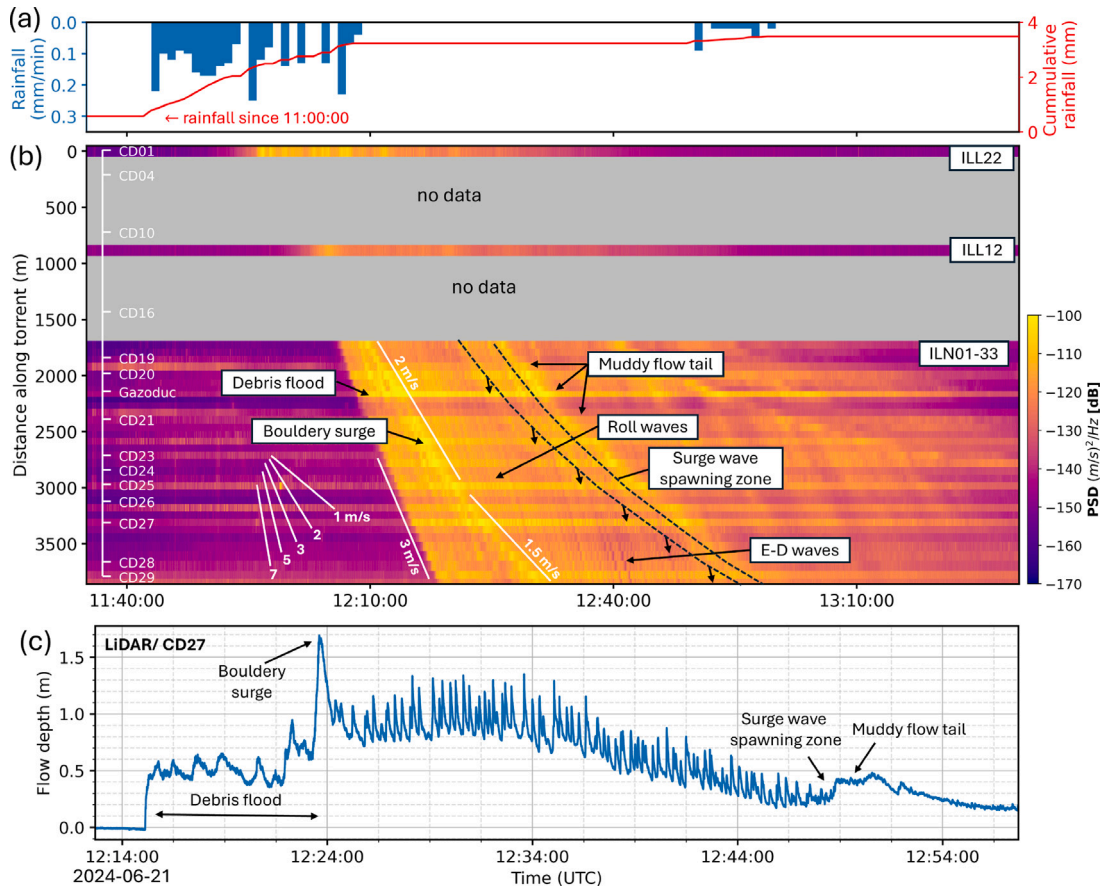


**Fig. 10.** Event 3: Time-distance visualization of debris flow recorded on 21 June 2024 at Illgraben. (a) Rainfall measured at CD1 in the catchment. (b) Spatiotemporal evolution of mean power spectral density (PSD) for all 35 seismic stations. Roll waves spawn in the flow tail and eventually evolve into erosion-deposition waves (E-D waves) below check dam CD27. (c) LiDAR based flow height measurement obtained at CD27.

all three recorded events, thus indicating that surge waves can form anywhere along the 2-km-long instrumented channel on the fan. Initial, small-scale flow perturbations are observed within the muddy flow tail on LiDAR-based hydrographs (Fig. 11) that rapidly transform into meter-scale surge wave trains, as shown by our distributed seismic measurements (Figs. 8–10). Those findings support the hypothesis that surge waves spontaneously emerge due to instabilities of the flowing material, as previously proposed by, e.g., Forterre and Pouliquen (2003), Viroulet et al. (2018), Edwards and Gray (2015) and Aaron et al. (2025).

We find that emergent wave trains evolve into two different branches: roll waves and erosion-deposition waves (Sections 4.2–4.3), as previously proposed by Edwards and Gray (2015) based on numerical simulations. We find two distinct wave-spawning mechanisms: (1) In the case of Event 2 and Event 3, we observe roll waves emerging out of thin, muddy flows, which fits into the classical picture of free-surface instabilities (e.g., Viroulet et al., 2018). In the case of Event 2, the roll waves transform into erosion-deposition waves as previously suggested by Edwards and Gray (2015) and Aaron et al. (2025) as the wave troughs fall below $h_{stop}$. (2) In Event 1 we observe the direct formation of erosion-deposition waves out of the flow tail, which to our knowledge had never been observed before in the context of debris flows. Detailed LiDAR-based hydrographs show small-scale flow undulations within the flow tail that abruptly grow into meter-scale erosion-deposition waves (Fig. 11d). Our data therefore suggest that there is an instability occurring near the static-flowing transition, as observed by Forterre and Pouliquen (2003) in lab-scale experiments on dry granular flows of sand and shown numerically by Edwards and Gray (2015). Furthermore, we propose that the formation of erosion-deposition waves, as observed in Event 1, is linked to the remobilization of static erodible material by the muddy flow tail, as previously shown for static erodible beds in the context of granular avalanches (Edwards et al., 2017; Rocha et al., 2019; Edwards et al., 2021).

### 5.2. Propagation of surge waves

Distributed seismic measurements allowed us to track erosion-deposition waves along the Illgraben torrent (Section 4.2), measure their velocity, and investigate their long-distance propagation characteristics which to our knowledge had never been observed with such high spatial resolution outside of laboratory-scale experiments (e.g. Daerr, 2001; Takagi et al., 2011; Edwards and Gray, 2015) and numerical simulations (Rocha et al., 2019). After spawning, erosion-deposition waves travel several kilometers along the Illgraben torrent, with constant wave-crest velocities between 3.5–6 m/s (Fig. 12). This was theoretically predicted for dry granular erosion-deposition waves as erosion and deposition are in balance (Edwards et al., 2017) forming steady avalanches, which propagate indefinitely along the torrent with constant velocity, as long as the erodible layer ahead of the wave does not change depth and the inclination remains the same (Edwards et al., 2017). Along the instrumented torrent section, the channel slope decreases from 4.5° to 3.5° and we hypothesize that this change is too small to produce a detectable decrease in velocity of erosion-deposition waves. Flow height measurements of erosion-deposition waves at check dam CD27 (Fig. 12a,b) further show correlations between the thickness of the erodible layer ($h_{stop}$), wave height ($A$) and wave velocity ($v_s$). Those findings indicate that large, fast erosion-deposition waves are found in debris flows that produce a thick erodible layer.

In case of Event 1 we observed a meter-thick static layer of erodible material (Fig. 7) that formed as the bulk flow came to rest and

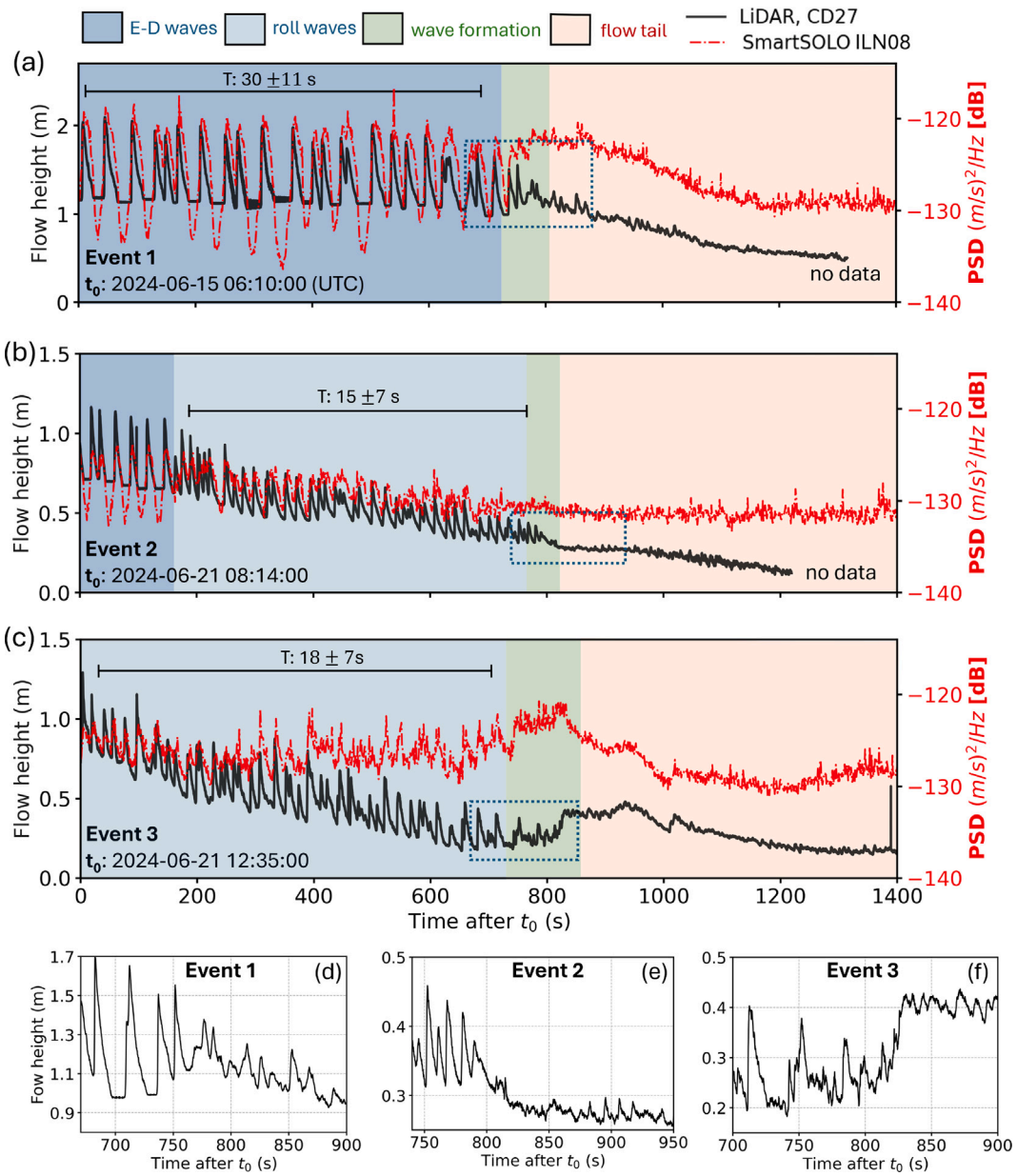


**Fig. 11.** Comparative analysis of seismic data (red lines, mean PSD 30–90 Hz) and LiDAR-based flow height measurements (black lines) at CD27. Surge waves emerge out of the flow tail in all three events. Average wave periods (T) are indicated for all three events. (a) Spawning of erosion-deposition waves (E-D waves) out of a meter thick flow tail. (b) and (c) Roll waves spawn out of a thinner flow tail (0.25 m). (d-f) Zoomed-in sections of (a-c, blue dashed box) highlighting the wave formation.

was periodically re-mobilized through traversing erosion-deposition waves. Similar observations were reported by Takagi et al. (2011) in laboratory-scale experiments, by Chen et al. (2024) in debris flows, and were described numerically by Rocha et al. (2019) for dry-granular flows, where periodic trains of erosion-deposition waves with similar sizes are observed propagating over an erodible layer with nearly constant thickness. Meter-scale erosion-deposition waves form within only hundreds of meters of flow distance (Fig. 8, Fig. 11a) as predicted by Edwards and Gray (2015), showing how surging debris flows can magnify the hazard potential of debris flows within short flow distances. In Event 2 the static layer decreases in thickness over time, which correlates with a decrease in wave velocity and wave size (Fig. 12c-g). We hypothesize that a gradual change in flow composition is responsible for the temporal change in stopping height ($h_{stop}$). We cannot further quantify the compositional change in flow material as the force plate at Illgraben (McArdell, 2016) was not operational for the investigated events and therefore no bulk densities were measured.

Observed erosion-deposition waves in Event 1 and Event 2 rarely overtake and merge since for the run-out distances within the Illgraben torrent the velocity differences between subsequent waves are too small and/or periods between waves are too large (Fig. 12a,b). This finding further indicates that erosion-deposition waves at Illgraben reach a steady traveling state, resulting in a periodic wave train in which subsequent waves have similar size and velocity and wave merging does not occur regularly. We note here that merging on smaller scales within the spawning zone is not resolved with our distributed seismic data, since amplitudes of small-scale surface undulations within the flow tail are too small and sensor spacing is too large. This is illustrated in Fig. 11, where small waves, leaving the spawning zone are not resolved in the seismic data but only visible in the flow height data.

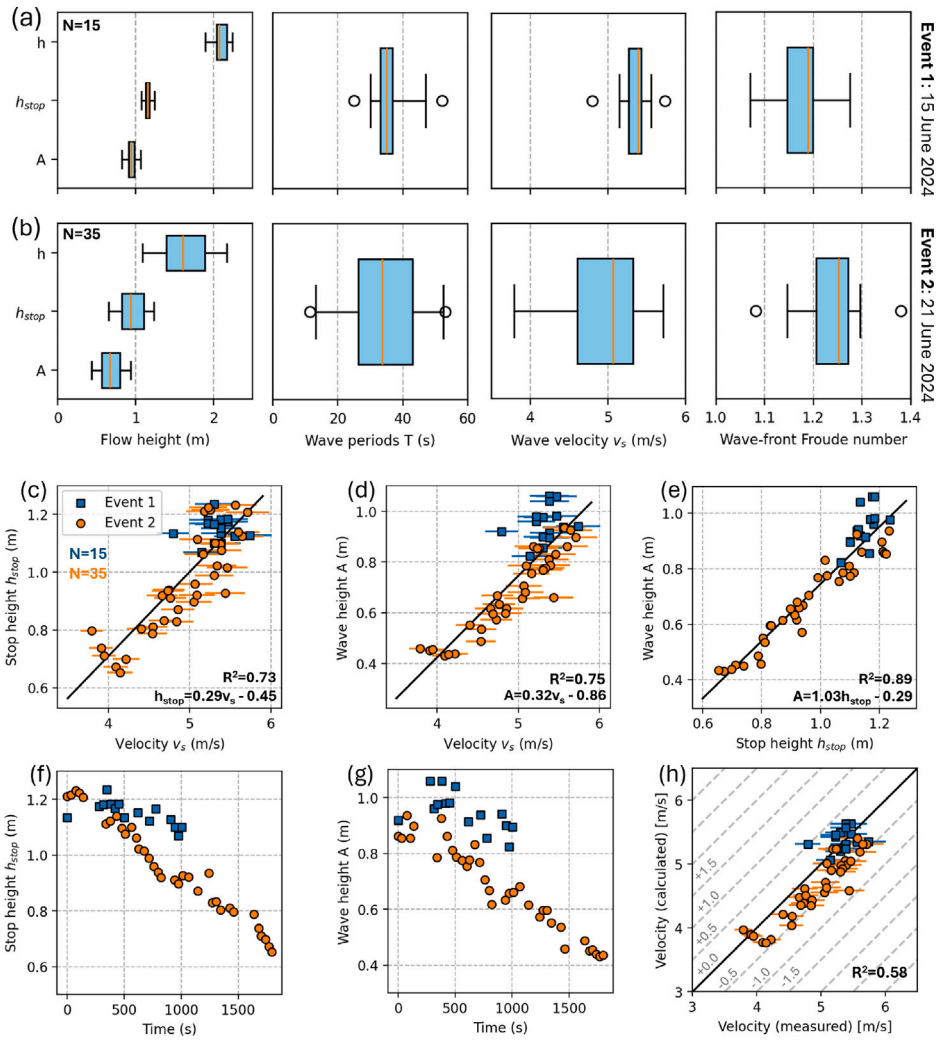


**Fig. 12.** Summary of key parameters of erosion-deposition waves from debris flows Event 1 and Event 2 measured between CD27 and CD28. (a, b) Boxplots of key characteristics of both debris flows. The center line shows the median of the data series, the edges of the box represent the lower and upper quartiles, the whiskers show the 1.5 x interquartile range, and the outliers are marked with o. (c-e) Relations between erosion-deposition wave front velocity $v_s$, stop height $h_{stop}$ and wave height A (black lines: linear fits). (e) Relation between $h_{stop}$ and $A$. (f, g) Temporal trends of stop height $h_{stop}$ and wave front velocity $v_s$ of subsequent erosion-deposition waves. (h) Comparison of measured erosion-deposition wave front velocities and calculated velocities based on Eq. (1).

### 5.3. Annihilation of surge waves

Surge waves are typically faster than the bulk flow (Spielmann et al., 2025) and also faster than debris flow fronts with bouldery composition as our data shows (Figs. 8–10). Surge waves spawning in the flow tail kilometers upstream of the front cross the flow body as roll waves (Event 3) or traverse the static erodible layer as erosion-deposition waves (Event 1 and Event 2) and merge with the debris flow front or during later event stages directly discharge into the Rhône River at the channel outlet (Fig. 9). We do not observe surge waves that traverse the debris flow front and continue flowing downstream but rather see that surge waves are stopped (annihilated) by debris flow fronts. Furthermore, in Event 1 we observed erosion-deposition waves that transform into roll waves (Fig. 8) as they travel along the channel, which to our knowledge was never observed before. We speculate that changes in flow composition lead to the transformation of erosion-deposition waves into roll waves, as static regions within the wave troughs disappear. This observation shows the close relation between roll waves and erosion-deposition waves, as roll waves can transform into erosion-deposition waves (Edwards and Gray, 2015; Aaron et al., 2025) and vice versa.

### 5.4. Implication for debris-flow hazard and engineering geology

Surge waves increase peak velocity and flow height of debris flows and momentarily accelerate immersed boulders (Spielmann et al., 2025). They therefore are more destructive than the continuous, slow moving flow from which they typically originate. Illgraben observations in 2024 (Section 4.2) furthermore show that single debris flows can produce up to 100 subsequent surge waves leading to repeated high impact loads (Hungr et al., 1984; Zeng and Cui, 2015) on bridge pillars, check dams and other infrastructure for up to hours, which promotes material fatigue and can ultimately cause structural failure.

The peak flow heights, peak discharge and elevated impact loads associated with surge waves must be considered in hazard management of debris flows. At the same time, the present study shows that check dam structures, which are typical engineering counter measures for debris flows, may be less effective for surge wave mitigation: Check dams reduce the kinetic energy of mountain streams by reducing the channel slope (Jaeggi and Pellandini, 1997) and stabilize the channel (McArdell and Sartori, 2020). A reduction in channel slope leads to reduced flow velocities and an increase in flow height according to mass conservation arguments. However, erosion-deposition wave velocities depend on flow height and channel slope (see Eq. (1)), as

well. The reduction of channel slope, which check dams provide, can lead to a reduction in flow velocities that cause conditions in favor of erosion-deposition waves. Apart from potential effects on surge wave formation, the check dams at Illgraben do not significantly slow down, let alone stop, surge waves. In all three investigated events, we observe surge waves that pass multiple, 3–5 m high, check dams along the 2 km long instrumented torrent section without notable velocity changes. Video footage (Video V5, Section 7) indicates that surge waves pass check dams and, in case of erosion-deposition waves, remobilize the static material below the check dam without altering wave velocities. Finally, the present study shows that surge waves form spontaneously and reach meter scale within only a few hundreds of meters. This "spawning zone" is small, yet the main contributor to flow dynamical complexity, and it moves downstream itself. Any engineering countermeasure therefore must be placed carefully along the debris flow runout to avoid missing surge wave formation.

## 6. Summary and conclusion

We used a near-torrent nodal array installed along the Illgraben catchment in Switzerland to obtain distributed seismic data from debris flows. We analyze three debris flows recorded in the summer months of 2024. Furthermore, we used flow height measurements as well as video material to support the interpretation of the seismic data. The main findings of our work can be summarized as follows:

1. Distributed seismic monitoring of debris flows resolves previously hidden flow patterns of large-scale surging behavior of debris flows as well as the formation of roll waves and erosion-deposition waves. Different boulder concentrations and flow velocities lead to measurable contrasts in seismic amplitudes that can be tracked along the torrent and thus allow debris flow mapping in time and space.
2. Erosion-deposition waves emerge (spawn) out of the flow tail, up to kilometers upstream of the front from where they travel with constant velocities (3.5–6 m/s) downstream, as predicted in laboratory-scale experiments (Rocha et al., 2019) and numerical simulations (Edwards et al., 2017). The spawning zone itself slowly migrates downstream, leading to surge wave arrivals that are sorted by distance: earlier arriving waves have their origin further upstream than later ones.
3. Erosion-deposition waves can grow to meter scales within only hundreds of meters of flow distance, as theoretically predicted by Edwards and Gray (2015) showing how surging debris flows can magnify the hazard potential within short torrent stretches. Furthermore, flow height data suggest that erosion-deposition wave height is related to the thickness of the erodible material within the channel and that therefore large waves can form in the presence of a thick erodible layer.
4. Check dams are unable to mitigate surge waves and do not significantly affect their propagation. Furthermore, check dams typically reduce the channel slope and therefore contribute to flow conditions, which are favorable for the formation of erosion-deposition waves.

The findings of this study provide novel insights into the surging behavior of debris flows. Surge wave formation is observed regularly in many catchments, and future studies should clarify whether the findings in this study also apply to other catchments.

## 7. Data and resources

Radar-based flow height measurements and precipitation measurements are accessible via http://dx.doi.org/10.16904/envidat.448. LiDAR-derived flow height measurements are accessible under https://doi.org/10.3929/ethz-c-000783019 and will be made available after the project end in February 2028 at this same site. The nodal dataset is collected under the International Federation of Digital Seismograph Networks (FDSN) network code 9S (Swiss Seismological Service (SED) at ETH Zurich, 2025) and is curated by the SED. The network information, with full metadata, is discoverable on European Integrated Data Archive (EIDA; http://eida-federator.ethz.ch/fdsnws/station/1/query?net=9S&format=text&station=ILN*&start=2024-01-01&end=2024-12-12). The data are currently restricted and will be made available after the project end in February 2028 at this same site. Timelapse video recordings of debris flows (10x speed) are accessible with following links: Video V1; https://doi.org/10.6084/m9.figshare.29320787.v1, Video V2; https://doi.org/10.6084/m9.figshare.29322494.v1, Video V3; https://doi.org/10.6084/m9.figshare.29322647.v1, Video V4, https://doi.org/10.6084/m9.figshare.29436134.v1 and Video V5; https://doi.org/10.6084/m9.figshare.30076306.v1.

## CRediT authorship contribution statement

**Christoph Wetter:** Writing – review & editing, Writing – original draft, Visualization, Methodology, Investigation. **Fabian Walter:** Writing – review & editing, Validation, Supervision, Project administration, Methodology, Funding acquisition, Conceptualization. **Brian W. McArdell:** Writing – review & editing, Validation, Supervision, Conceptualization. **Felix Blumenschein:** Writing – review & editing, Data curation, Conceptualization. **Raffaele Spielmann:** Writing – review & editing, Data curation. **Jordan Aaron:** Writing – review & editing, Data curation. **J.M.N.T. Gray:** Writing – review & editing, Conceptualization. **Anne Obermann:** Data curation, Resources. **Andreas Fichtner:** Writing – review & editing, Supervision, Project administration, Methodology, Conceptualization.

## Declaration of competing interest

The authors declare the following financial interests/personal relationships which may be considered as potential competing interests: Christoph Wetter reports financial support was provided by Swiss National Science Foundation (SNSF). Jordan Aaron reports financial support was provided by Swiss National Science Foundation (SNSF). J.M.N.T. Gray reports financial support was provided by Natural Environment Research Council (NERC). If there are other authors, they declare that they have no known competing financial interests or personal relationships that could have appeared to influence the work reported in this paper.

## Acknowledgments

This work was funded by the Swiss National Science Foundation (SNSF) Grant 00021_215631/1. LiDAR installations at Illgraben are funded by Swiss National Science Foundation (SNSF) Ambizione Grant 193081. J.M.N.T. Gray was supported by funding from Natural Environment Research Council (NERC) grants NE/X00029X/1 and NE/X013936/1. 35 SmartSolo seismic nodes were provided by ETH Zürich. The authors thank Dr. Johannes Aichele from ETH Zürich for his help with data curation. The authors also thank Dr. Jake Langham from the University of Manchester for his insightful comments. The authors are grateful for technical support and scientific advice from Dr. Alexandre Badoux (WSL), Dr. Zhen Zang (WSL/CUHK), Tobias Christ (WSL), Christoph Graf (WSL) and Stefan Boss (WSL). The authors are grateful to the Editor, Paolo Frattini, and the Guest Editor, Alessandro Leonardi, for their coordination, as well as two anonymous reviewers for their constructive feedback that significantly improved this manuscript.

## Appendix A. Supplementary data

Supplementary material related to this article can be found online at https://doi.org/10.1016/j.enggeo.2026.108648.

## References


Aaron, J., Langham, J., Spielmann, R., Hirschberg, J., McArdell, B., Boss, S., Johnson, C.G., Gray, J.M.N.T., 2025. Detailed observations reveal the genesis and dynamics of destructive debris-flow surges. Commun. Earth Environ. 6, 556. http://dx.doi.org/10.1038/s43247-025-02488-7.

Aaron, J., Spielmann, R., McArdell, B.W., Graf, C., 2023. High-frequency 3D LiDAR measurements of a debris flow: A novel method to investigate the dynamics of full-scale events in the field. Geophys. Res. Lett. 50 (5), http://dx.doi.org/10.1029/2022GL102373.

Allstadt, K.E., Farin, M., Iverson, R.M., Obryk, M.K., Kean, J.W., Tsai, V.C., Rapstine, T.D., Logan, M., 2020. Measuring basal force fluctuations of debris flows using seismic recordings and empirical green's functions. J. Geophys. Res.: Earth Surf. 125 (9), http://dx.doi.org/10.1029/2020JF005590, e2020JF005590.

Arai, M., Huebl, J., Kaitna, R., 2013. Occurrence conditions of roll waves for three grain–fluid models and comparison with results from experiments and field observation. Geophys. J. Int. 195 (3), 1464–1480. http://dx.doi.org/10.1093/gji/ggt352.

Arattano, M., Moia, F., 1999. Monitoring the propagation of a debris flow along a torrent. Hydrol. Sci. J. 44 (5), 811–823. http://dx.doi.org/10.1080/02626669909492275.

Badoux, A., Graf, C., Rhyner, J., Kuntner, R., McArdell, B., 2009. A debris-flow alarm system for the alpine illgraben catchment: Design and performance. Nat. Hazards 49, 517–539. http://dx.doi.org/10.1007/s11069-008-9303-x.

Balmforth, N.J., Liu, J.J., 2004. Roll waves in mud. J. Fluid Mech. 519, 33–54. http://dx.doi.org/10.1017/S0022112004000801.

Belli, G., Marchetti, E., Walter, F., Gheri, D., 2025. Infrasound unmasks flow turbulence as an additional seismic source in debris flows. Geophys. Res. Lett. 52 (8), http://dx.doi.org/10.1029/2025GL116107, e2025GL116107.

Belli, G., Walter, F., McArdell, B., Gheri, D., Marchetti, E., 2022. Infrasonic and seismic analysis of debris-flow events at illgraben (Switzerland): Relating signal features to flow parameters and to the seismo-acoustic source mechanism. J. Geophys. Res.: Earth Surf. 127, http://dx.doi.org/10.1029/2021JF006576.

Berti, M., Genevois, R., Lahusen, R., Simoni, A., Tecca, P., 2000. Debris flow monitoring in the acquabona watershed on the dolomites (Italian alps). Phys. Chem. Earth, Part B: Hydrol. Ocean. Atmosphere 25, 707–715. http://dx.doi.org/10.1016/S1464-1909(00)00090-3.

Chen, Q., Song, D., Chen, X., Feng, L., Li, X., Zhao, W., Zhang, Y., 2024. The erosion pattern and hidden momentum in debris-flow surges revealed by simple hydraulic jump equations. Water Resour. Res. 60 (11), http://dx.doi.org/10.1029/2023WR036090, e2023WR036090.

Chmiel, M., Walter, F., Wenner, M., Zhang, Z., McArdell, B., Hibert, C., 2021. Machine learning improves debris flow warning. Geophys. Res. Lett. 48, http://dx.doi.org/10.1029/2020GL090874.

Costa, J.E., Williams, G.P., 1984. Debris-flow dynamics. http://dx.doi.org/10.3133/ofr84606, URL https://www.youtube.com/watch?v=1qjV–hyXqo&t=1298s. (Accessed 21 August 2025).

Coviello, V., Arattano, M., Comiti, F., Macconi, P., Marchi, L., 2019. Seismic characterization of debris flows: Insights into energy radiation and implications for warning. J. Geophys. Res.: Earth Surf. 124 (6), 1440–1463. http://dx.doi.org/10.1029/2018JF004683.

Daerr, A., 2001. Dynamical equilibrium of avalanches on a rough plane. Phys. Fluids 13 (7), 2115–2124. http://dx.doi.org/10.1063/1.1377864.

Dressler, R.F., 1949. Mathematical solution of the problem of roll-waves in inclined opel channels. Comm. Pure Appl. Math. 2 (2–3), 149–194. http://dx.doi.org/10.1002/cpa.3160020203.

Edwards, A.N., Gray, J.M.N.T., 2015. Erosion–deposition waves in shallow granular free-surface flows. J. Fluid Mech. 762, 35–67. http://dx.doi.org/10.1017/jfm.2014.643.

Edwards, A.N., Russell, A.S., Johnson, C.G., Gray, J.M.N.T., 2019. Frictional hysteresis and particle deposition in granular free-surface flows. J. Fluid Mech. 875, 1058–1095. http://dx.doi.org/10.1017/jfm.2019.517.

Edwards, A.N., Viroulet, S., Johnson, C.G., Gray, J.M.N.T., 2021. Erosion-deposition dynamics and long distance propagation of granular avalanches. J. Fluid Mech. 915, A9. http://dx.doi.org/10.1017/jfm.2021.34.

Edwards, A.N., Viroulet, S., Kokelaar, B.P., Gray, J.M.N.T., 2017. Formation of levees, troughs and elevated channels by avalanches on erodible slopes. J. Fluid Mech. 823, 278–315. http://dx.doi.org/10.1017/jfm.2017.309.

Farin, M., Mangeney, A., Roche, O., 2014. Fundamental changes of granular flow dynamics, deposition, and erosion processes at high slope angles: Insights from laboratory experiments. J. Geophys. Res.: Earth Surf. 119 (3), 504–532. http://dx.doi.org/10.1002/2013JF002750.

Farin, M., Tsai, V.C., Lamb, M.P., Allstadt, K.E., 2019. A physical model of the high-frequency seismic signal generated by debris flows. Earth Surf. Process. Landf. 44 (13), 2529–2543. http://dx.doi.org/10.1002/esp.4677.

Forterre, Y., 2006. Kapiza waves as a test for three-dimensional granular flow rheology. J. Fluid Mech. 563, 123–132. http://dx.doi.org/10.1017/S0022112006001509.

Forterre, Y., Pouliquen, O., 2003. Long-surface-wave instability in dense granular flows. J. Fluid Mech. 486, 21–50. http://dx.doi.org/10.1017/S0022112003004555.

Fraccarollo, L., Papa, M., 2000. Numerical simulation of real debris-flow events. Phys. Chem. Earth, Part B: Hydrol. Ocean. Atmosphere 25 (9), 757–763. http://dx.doi.org/10.1016/S1464-1909(00)00098-8.

Gray, J.M.N.T., Edwards, A.N., 2014. A depth-averaged $\mu(I)$-rheology for shallow granular free-surface flows. J. Fluid Mech. 755, 503–534. http://dx.doi.org/10.1017/jfm.2014.450.

Guo, X., Li, Y., Cui, P., Yan, H., Zhuang, J., 2020. Intermittent viscous debris flow formation in jiangjia gully from the perspectives of hydrological processes and material supply. J. Hydrol. 589, 125184. http://dx.doi.org/10.1016/j.jhydrol.2020.125184.

Hirschberg, J., Badoux, A., McArdell, B.W., Leonarduzzi, E., Molnar, P., 2021. Evaluating methods for debris-flow prediction based on rainfall in an alpine catchment. Nat. Hazards Earth Syst. Sci. 21 (9), 2773–2789. http://dx.doi.org/10.5194/nhess-21-2773-2021.

Hua, J., Wu, M., Mulholland, J., Neelin, J., Tsai, V., Trugman, D., 2023. High-resolution precipitation monitoring with a dense seismic nodal array. Sci. Rep. 13, http://dx.doi.org/10.1038/s41598-023-38008-w.

Hungr, O., Morgan, G.C., Kellerhals, R., 1984. Quantitative analysis of debris torrent hazards for design of remedial measures. Can. Geotech. J. 21 (4), 663–677. http://dx.doi.org/10.1139/t84-073.

Hürlimann, M., Rickenmann, D., Graf, C., 2003. Field and monitoring data of debris-flow events in the swiss alps. Can. Geotech. J. 40 (1), 161–175. http://dx.doi.org/10.1139/t02-087.

Iverson, R.M., 2012. Elementary theory of bed-sediment entrainment by debris flows and avalanches. J. Geophys. Res.: Earth Surf. 117 (F3), http://dx.doi.org/10.1029/2011JF002189.

Iverson, R., Reid, M., Lahusen, R., 1997. Debris-flow mobilization from landslides. Annu. Rev. Earth Planet. Sci. 25, 85–138. http://dx.doi.org/10.1146/annurev.earth.25.1.85.

Jaeggi, M.N.R., Pellandini, S., 1997. Torrent check dams as a control measure for debris flows. In: Recent Developments on Debris Flows. Springer Berlin Heidelberg, pp. 186–207. http://dx.doi.org/10.1007/BFb0117769.

Jeffreys, H., 1925. The flow of water in an inclined channel of rectangular section. Lond. Edinb. Dublin Philos. Mag. J. Sci. 49 (293), 793–807. http://dx.doi.org/10.1080/14786442508634662.

Johnson, C.G., Kokelaar, B.P., Iverson, R.M., Logan, M., LaHusen, R.G., Gray, J.M.N.T., 2012. Grain-size segregation and levee formation in geophysical mass flows. J. Geophys. Res.: Earth Surf. 117 (F1), http://dx.doi.org/10.1029/2011JF002185.

Kean, J.W., McCoy, S.W., Tucker, G.E., Staley, D.M., Coe, J.A., 2013. Runoff-generated debris flows: Observations and modeling of surge initiation, magnitude, and frequency. J. Geophys. Res.: Earth Surf. 118 (4), 2190–2207. http://dx.doi.org/10.1002/jgrf.20148.

Kokelaar, B.P., Bahia, R.S., Joy, K.H., Viroulet, S., Gray, J.M.N.T., 2017. Granular avalanches on the moon: Mass-wasting conditions, processes, and features. J. Geophys. Res.: Planets 122 (9), 1893–1925. http://dx.doi.org/10.1002/2017JE005320.

Lai, V.H., Tsai, V.C., Lamb, M.P., Ulizio, T.P., Beer, A.R., 2018. The seismic signature of debris flows: Flow mechanics and early warning at Montecito, california. Geophys. Res. Lett. 45 (11), 5528–5535. http://dx.doi.org/10.1029/2018GL077683.

Li, X., Sovilla, B., Gray, J.M.N.T., Gaume, J., 2024. Transient wave activity in snow avalanches is controlled by entrainment and topography. Commun. Earth Environ. 5 (1), 77. http://dx.doi.org/10.1038/s43247-023-01157-xx.

Mangeney, A., Roche, O., Hungr, O., Mangold, N., Faccanoni, G., Lucas, A., 2010. Erosion and mobility in granular collapse over sloping beds. J. Geophys. Res.: Earth Surf. 115 (F3), http://dx.doi.org/10.1029/2009JF001462.

Marchetti, E., Walter, F., Barfucci, G., Genco, R., Wenner, M., Ripepe, M., McArdell, B.W., Price, C., 2019. Infrasound array analysis of debris flow activity and implication for early warning. J. Geophys. Res.: Earth Surf. 124 (2), 567–587. http://dx.doi.org/10.1029/2018JF004785.

McArdell, B.W., 2016. Field measurements of forces in debris flows at the illgraben: Implications for channel-bed erosion. Int. J. Eros. Control. Eng. 9 (4), 194–198. http://dx.doi.org/10.13101/ijece.9.194.

McArdell, B.W., Bartelt, P., Kowalski, J., 2007. Field observations of basal forces and fluid pore pressure in a debris flow. Geophys. Res. Lett. 34 (7), http://dx.doi.org/10.1029/2006GL029183.

McArdell, B.W., Sartori, M., 2020. The illgraben torrent system. In: Landscapes and Landforms of Switzerland,Year=2021. Springer International Publishing, Cham, pp. 367–378. http://dx.doi.org/10.1007/978-3-030-43203-4_25.

Missbauer, P., 1971. Stuetzmauer für die wildbachverbauung im illgraben. Schweiz. Bauztg., 89 (1971) 1003–1006. http://dx.doi.org/10.5169/SEALS-85002.

Mostbauer, K., Kaitna, R., Prenner, D., Hrachowitz, M., 2018. The temporally varying roles of rainfall, snowmelt and soil moisture for debris flow initiation in a snow-dominated system. Hydrol. Earth Syst. Sci. 22 (6), 3493–3513. http://dx.doi.org/10.5194/hess-22-3493-2018.

Navratil, O., Liébault, F., Bellot, H., Travaglini, E., Theule, J., Chambon, G., Laigle, D., 2013. High-frequency monitoring of debris-flow propagation along the Réal Torrent, Southern French Prealps. Geomorphology 201, 157–171. http://dx.doi.org/10.1016/j.geomorph.2013.06.017.

Ouster, 2025. OS1–128. URL https://data.ouster.io/downloads/datasheets/datasheet-rev7-v3p1-os1.pdf. (Accessed: 19 May 2025).

Razis, D., Edwards, A.N., Gray, J.M.N.T., van der Weele, K., 2014. Arrested coarsening of granular roll waves. Phys. Fluids 26 (12), 123305. http://dx.doi.org/10.1063/1.4904520.

Rocha, F.M., Johnson, C.G., Gray, J.M.N.T., 2019. Self-channelisation and levee formation in monodisperse granular flows. J. Fluid Mech. 876, 591–641. http://dx.doi.org/10.1017/jfm.2019.518.

Schlunegger, F., Badoux, A., McArdell, B.W., Gwerder, C., Schnydrig, D., Rieke-Zapp, D., Molnar, P., 2009. Limits of sediment transfer in an alpine debris-flow catchment, Illgraben, Switzerland. Quat. Sci. Rev. 28, 1097–1105. http://dx.doi.org/10.1016/j.quascirev.2008.10.025.

Schöffl, T., Nagl, G., Koschuch, R., Schreiber, H., Hübl, J., Kaitna, R., 2023. A perspective of surge dynamics in natural debris flows through pulse-Doppler radar observations. J. Geophys. Res.: Earth Surf. 128 (9), http://dx.doi.org/10.1029/2023JF007171, e2023JF007171.

Spielmann, R., Aaron, J., 2024. A new method for detailed discharge and volume measurements of debris flows based on high-frequency 3D LiDAR point clouds; Illgraben, Switzerland. Eng. Geol. 329, 107386. http://dx.doi.org/10.1016/j.enggeo.2023.107386.

Spielmann, R., Schöffl, T., Kaitna, R., Aaron, J., 2025. Sorting and surging: 3D LiDAR and pulse-Doppler radar analysis of a natural debris flow. J. Geophys. Res.: Earth Surf. 130 (11), http://dx.doi.org/10.1029/2025JF008450, e2025JF008450.

Swiss Seismological Service (SED) at ETH Zurich, 2025. Temporary deployments in Switzerland associated with landslides. http://dx.doi.org/10.12686/SED/NETWORKS/XP.

Takagi, D., McElwaine, J.N., Huppert, H.E., 2011. Shallow granular flows. Phys. Rev. E 83, 031306. http://dx.doi.org/10.1103/PhysRevE.83.031306.

Trowbridge, J.H., 1987. Instability of concentrated free surface flows. J. Geophys. Res.: Ocean. 92 (C9), 9523–9530. http://dx.doi.org/10.1029/JC092iC09p09523.

Tsai, V.C., Minchew, B., Lamb, M.P., Ampuero, J.-P., 2012. A physical model for seismic noise generation from sediment transport in rivers. Geophys. Res. Lett. 39 (2), http://dx.doi.org/10.1029/2011GL050255.

Vega, 2025. Vegaplus C 22 radar. URL https://www.vega.com/de-ch/produkte/produktkatalog/fuellstand/radar/vegapuls-c-22.

Viroulet, S., Baker, J.L., Rocha, F.M., Johnson, C.G., Kokelaar, B., Gray, J.M.N.T., 2018. The kinematics of bidisperse granular roll waves. J. Fluid Mech. 848, 836–875. http://dx.doi.org/10.1017/jfm.2018.348.

Zanuttigh, B., Lamberti, A., 2007. Instability and surge development in debris flows. Rev. Geophys. 45 (3), http://dx.doi.org/10.1029/2005RG000175.

Zeng, C., Cui, Z.e.a., 2015. Failure modes of reinforced concrete columns of buildings under debris flow impact. Landslides 12, 561–571. http://dx.doi.org/10.1007/s10346-014-0490-0.

Zhang, Z., Walter, F., McArdell, B.W., de Haas, T., Wenner, M., Chmiel, M., He, S., 2021a. Analyzing bulk flow characteristics of debris flows using their high frequency seismic signature. J. Geophys. Res.: Solid Earth 126 (12), http://dx.doi.org/10.1029/2021JB022755.

Zhang, Z., Walter, F., McArdell, B.W., Wenner, M., Chmiel, M., de Haas, T., He, S., 2021b. Insights from the particle impact model into the high-frequency seismic signature of debris flows. Geophys. Res. Lett. 48 (1), http://dx.doi.org/10.1029/2020GL088994.